Protection of In-River Hydrokinetic Power-Generating Devices from Surface Debris in Alaskan Rivers

Prepared by

J. B. Johnson, J. Schmid, J. Kasper, A. C. Seitz, P. Duvoy

Alaska Center for Energy and Power,
Alaska Hydrokinetic Energy Research Center
University of Alaska Fairbanks

September 2014

ACEP
Alaska Center for Energy and Power

UAF
UNIVERSITY OF ALASKA FAIRBANKS

Cover photo – Direct debris impact test on the AHERC research debris diversion platform. Photo credit – Todd Paris

Acknowledgments

This project would not have been possible without the direct and indirect support of many people and organizations. The work was conducted under subcontract to Alaska Power and Telephone, with funding from the Denali Commission under grant number 01198-00-UAF G6078. We thank Ben Beste, Alaska Power and Telephone, and the Denali Commission for their support. The City of Nenana and the Nenana Tribal Council provided encouragement, land to stage project efforts, and accommodation facilities. Charlie Hnilicka, Inland Barge Service, and Matt Sweetsir, Ruby Marine, Inc., provided on-river barge assistance. Jon's Machine Shop provided design, engineering, and fabricating services, and Mark Evans and Parker Bradley helped with log wrangling and fisheries studies.

Contents

List of Figures

List of Tables

Executive Summary

In spring 2010, Alaska Power and Telephone (AP&T) deployed a 25 kW New Energy Corporation EnCurrent hydrokinetic turbine in the Yukon River at Eagle, Alaska, to determine the feasibility of using river in-stream energy conversion (RISEC) devices to supply power to remote communities. The turbine was deployed on a floating platform and operated successfully until problems with surface and submerged debris caused AP&T to end operations. The company found that extensive debris problems on the Yukon at Eagle posed a severe challenge to operating the turbine and created significant safety hazards for their personnel. As a result, plans for deploying the turbine in 2011 were cancelled, and AP&T initiated a project with the Alaska Hydrokinetic Research Center (AHERC) to examine ways to reduce the hazard of surface debris for RISEC devices deployed from floating platforms.

The focus of AHERC's study was on the characteristics of river debris and strategies for reducing the impact of debris on RISEC infrastructure. This information was used to develop statistics on the occurrence of debris at AHERC's Tanana River Test Site located in Nenana, Alaska, and to design a research debris diversion platform (RDDP). The RDDP consists of two steel pontoons joined in a wedge with its apex facing upstream (Figure E1a). A vertical-axis freely rotating cylinder (1.1 m diameter) was placed at the leading edge of the wedge. The rotating cylinder initially employed an array of hinged vanes that would exploit the river current to promote rotation, but later was covered with plastic to reduce surface friction. The angle between the two pontoons of the RDDP is adjustable, from 25 to 77 degrees, and the rotating cylinder at the leading edge may be replaced with a fixed angled (62°) wedge (Figure E1b).

a b

Figure E1. RDDP in its closed position showing the debris sweep with hinged vanes (a) and the RDDP front-end mount shown separately from the plastic-covered angled front end and the plastic-covered debris sweep cylinder (b).

The RDDP was moored to a buoy that was connected by a chain to an embedment anchor. The buoy anchor chain was the only tether that traversed the full depth of the river. The tether from the RDDP to the buoy ran parallel to the river surface. This mooring arrangement reduced the probability that debris would catch on mooring tether lines. Any debris that caught on the anchor chain would have a limited effect on RISEC device performance. Tests

of the RDDP's ability to divert debris around a protected zone and the RDDP's effect on river turbulence were conducted at AHERC's Tanana River Test Site.

The RDDP system (i.e., anchor, buoy, tether line, RDDP) using the cylindrical debris sweep performed well at diverting river surface debris around the RDDP. Debris impact forces on the RDDP ranged from 3 kN to over 6 kN during the study period. The sharp-angled front end (Figure E1b) did divert debris, but was much less effective than the debris sweep. The mooring buoy's constant movement caused by river turbulence created an unstable site for debris to accumulate, and the buoy's large buoyancy made it difficult for debris to override the buoy. The mooring buoy provided a strong first defense against surface debris by reorienting the debris lengthwise, parallel to the current flow direction, making it easier for the RDDP to divert debris.

Any effect of the RDDP on river turbulence was masked by the considerable, natural variability of the river flow. Quasi-stationary acoustic Doppler current profiler (ADCP) measurements detected a decrease in the northward directed near-surface river velocities as well as an increase in the westward directed near-surface velocities in the RDDP's wake. These changes were attributed to the presence of the RDDP. Changes in river flow direction were negligible several meters downstream from the RDDP.

The opening angle between the RDDP pontoons has a significant effect on the ability of the pontoons to divert debris around the RDDP. The water current force that acts to clear debris from the pontoon surfaces decreases with pontoon opening angle, while the water force acting to pin debris to the pontoon increases with pontoon opening angle. Debris can become pinned against the RDDP when the opening angle of the pontoons is greater than about 58 degrees. Larger opening angles can result in debris counter-rotating (rotating counterclockwise with respect to the river's right bank) under the RDDP.

High-momentum debris impacts against the RDDP can cause it to rotate about its mooring anchor point, allowing debris to move into the "protected" river current flow path behind the RDDP. To reduce this effect the RDDP should be connected to the downstream RISEC floating platform, such that the combined inertia of the RDDP and the RISEC platform acts to resist the debris impact momentum.

The performance of the RDDP can be improved by covering its pontoon surfaces with a hard plastic sheet to reduce friction and thus provide a smooth contact surface for debris. Moving the safety railing from the outside to the inside of the pontoons will reduce the probability of a debris object branch catching on a railing stanchion. Reducing the inertia of the RDDP debris sweep and operating the RDDP with a pontoon opening angle of less than 40 degrees will improve the RDDP's ability to clear debris from the front of the RDDP and divert the debris. Increasing the RDDP pontoon draft will reduce the probability of debris counter-rotating under the pontoon.

The RDDP system can provide effective protection from river surface debris for RISEC devices deployed from a floating platform. The RDDP is not designed to divert subsurface debris that is moving in the river. Further work is needed in understanding the prevalence of subsurface debris to determine the probability of subsurface debris impact on a RISEC device and to guide concepts for protecting RISIC devices from subsurface debris.

Introduction

In spring 2010, Alaska Power and Telephone (AP&T) installed a 25 kW New Energy Corporation EnCurrent hydrokinetic turbine generator in the Yukon River at Eagle, Alaska, as a pilot study to determine the feasibility of using river in-stream energy conversion (RISEC) devices to supply power to remote communities (Figure 1a). The turbine, which was deployed on a floating platform, operated successfully until July, when surface debris piled up in front of the turbine barge (Figure 1b), and large submerged debris damaged the barge's mooring equipment. After repairs, the turbine was redeployed in August and operated until a second debris event consisting of both surface and submerged debris damaged the turbine power cable in mid-August, causing AP&T to end operations. During periods of operation, the turbine performed well and supplied power to the power grid at Eagle (Johnson and Pride 2010; Johnson et al. 2013).

a b

Figure 1. New Energy 25 kW hydrokinetic power turbine on the Yukon River at Eagle, Alaska, August 2010 (photo credit: J. Johnson) (a) and debris accumulation in front of the turbine barge (photo credit: Alaska Power & Telephone) (Johnson and Pride 2010; Johnson et al. 2013).

Alaska Power and Telephone found that the extensive debris problems on the Yukon at Eagle posed a severe challenge to operating the turbine and created significant safety hazards for personnel. As a result, plans for deploying the turbine in 2011 were cancelled, and AP&T initiated a project with the Alaska Hydrokinetic Research Center (AHERC) to examine ways to reduce the hazard of surface debris for surface-mounted hydrokinetic devices.

The primary area of interest was development of a way to divert river surface debris around a RISEC device to prevent clogging or damage to surface-deployed RISEC devices. The AHERC debris mitigation study was conducted in five phases:

1. Reviewing the characteristics of river surface debris and strategies used to reduce the impact of debris on river infrastructure (Tyler 2011).
2. Designing and building a research debris diversion platform (RDDP) using information from the review. The RDDP was designed to have adjustable pontoon angles and accommodate different nose configurations at its apex.
3. Analyzing the mechanics of debris diversion to determine the important factors that control the effectiveness of the RDDP (Johnson et al. 2013).
4. Conducting full-scale tests of the RDDP's effectiveness at diverting debris by impacting the RDDP with full-scale log debris. The purpose of building the RDDP

and then conducting tests using full-scale logs was to determine empirically the important factors controlling RDDP debris diversion performance and to measure debris impact loads on the RDDP. The tests were also used to validate the analytical evaluation of the important factors controlling RDDP performance derived by Johnson et al. (2013).

5. Conducting long-term deployments of the RDDP to observe its response to the natural river debris environment.

Tests of the RDDP were conducted during the summers of 2011 and 2012 at AHERC's Tanana River Test Site (TRTS) located at Nenana, Alaska. River debris characteristics, debris mitigation strategies, and TRTS characterization studies are described in Tyler (2011) and Johnson et al (2013). The following sections of this report describe the design, construction, and testing of the RDDP. Test results were used to identify features of debris diversion platforms that increase their ability to shed debris and provide increased protection of surface deployed RISEC devices.

Study Location and Previous Work

The TRTS is located on the Tanana River at Nenana, Alaska, and has been under development since 2008 when the first characterization studies were performed (Figure 2). Testing was conducted in the upper reach of the river at the point marked in Figure 2 as the mooring buoy.

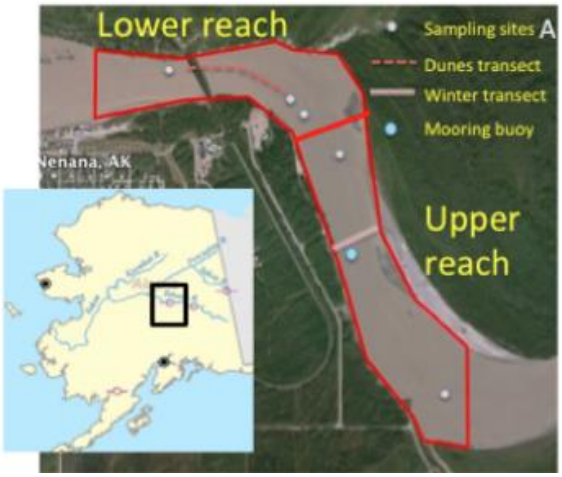

Figure 2. Tanana River Test Site site location map.

Characterization studies of the TRTS focused on determining the test site's bathymetry, current velocity and turbulence, seasonal variation in hydrokinetic power, sediment transport, fish populations, and prevalence of debris in the river. Major findings are that current velocities have significant seasonal variation, the river transports large volumes of suspended and bed load sediment, and smolt (whose well-being is of high concern to river stakeholders) primarily travel in the thalweg in May and June. The highest volumes of debris occur in early summer, immediately after ice breakup, or during periods of high discharge. River current velocities range from more than 2 m/s in the summer to less than 0.8 m/s during the winter. These characteristics result in a substantial difference in hydrokinetic power, as power is proportional to the cube of velocity. The highest power density with the least amount of turbulence occurs in long straight reaches of the river that have little change in bathymetry. River bends and sections of river with significant changes in bathymetry exhibit higher turbulence than straight sections of rivers (Figure 3).

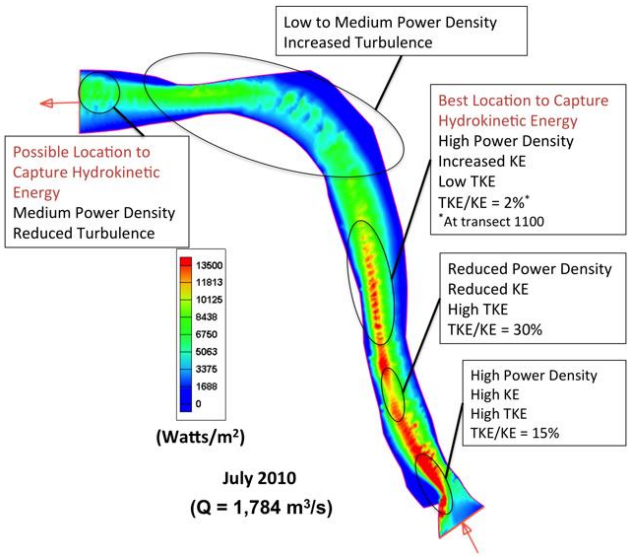

Figure 3. Power density at the Tanana River Test Site, with notations about turbulence and placement of RISEC devices (Johnson et al. 2013, modified from Duvoy and Toniolo 2012).

River debris at the TRTS occurs throughout the open-water season, but is highest immediately after breakup and during periods of rising stage (although no strong correlation was found to exist between debris and river stage, Figure 4). River discharge and stage are directly related, such that increasing stage means the discharge is increasing. The association of debris and river stage is complex, in that debris is deposited on sandbars and riverbanks during periods of decreasing stage and then refloated when the stage next increases. There appears to be a period of decreased debris flow after major debris events (irrespective of river stage), which may indicate that debris has been cleared from the system for a time while bank erosion and other factors reload the river system with new debris.

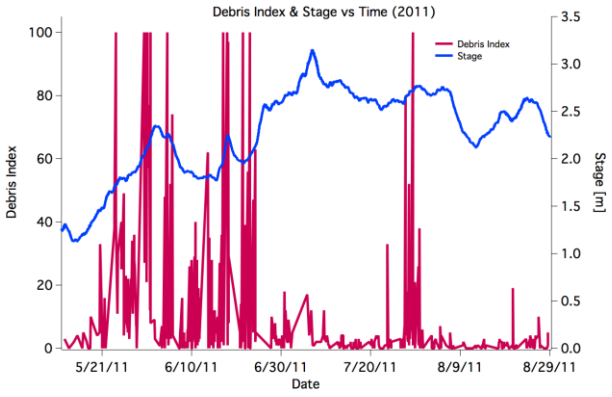

Figure 4. Debris index. Debris was counted for 5-minute periods every hour or until 100 debris pieces passed the observation (redrafted from Johnson et al. 2013).

Study Approach

The focus of this study was on (1) designing, constructing, and testing the RDDP to determine how best to deflect debris around a deployed RISEC device, and (2) determining the frequency and location of surface debris in the river. The RDDP design was developed using information from a review of debris characteristics and methods to mitigate the effects of river debris on infrastructure (Tyler 2011) and on the experiences of demonstration projects at Ruby and Eagle, Alaska, and Ft. Simpson, Yukon, with debris (Johnson and Pride

2010; Johnson et al. 2013). A solar/battery-powered time-lapse camera system was developed and installed on the shore at the TRTS to observe floating debris.

Debris diversion structures were placed in front of the RISEC devices during part of the demonstration RISEC device deployments at Ruby, Eagle, and Ft. Simpson. These structures generally consisted of floating wooden beams connected at one end, with the opposite end opened at a set angle to divert debris. The apex of the debris diversion boom faced upstream. While these devices did deflect some debris, debris was observed to hang up on the apex of the diverters and roll under the debris diverters. In some cases, the debris was submerged and damaged a turbine blade on impact or caught on an electrical cable running to shore (Johnson et al. 2013; Johnson and Pride 2010). A systematic consideration of the expected debris-impact forces, the influence of diversion device opening angle, and friction between the diversion device and debris are often not accounted for when designing debris diversion devices. The RDDP design developed for this study is intended to allow for a systematic investigation of the factors that influence the effectiveness of a debris diversion device under different configurations that include varying the opening angle, friction reduction, and front-end geometry.

RDDP Design and Construction

Design Analysis

Of the variety of possible debris mitigation technologies reviewed by Tyler (2011), the most practical method for sustained operations appears to be developing a way to divert river debris around the floating platform that supports a RISEC device. Typically, this diversion system consists of two floating booms joined at their upstream end and deployed at an angle sufficiently wide to protect a RISEC device barge deployed downstream from the diversion boom (Figure 5).

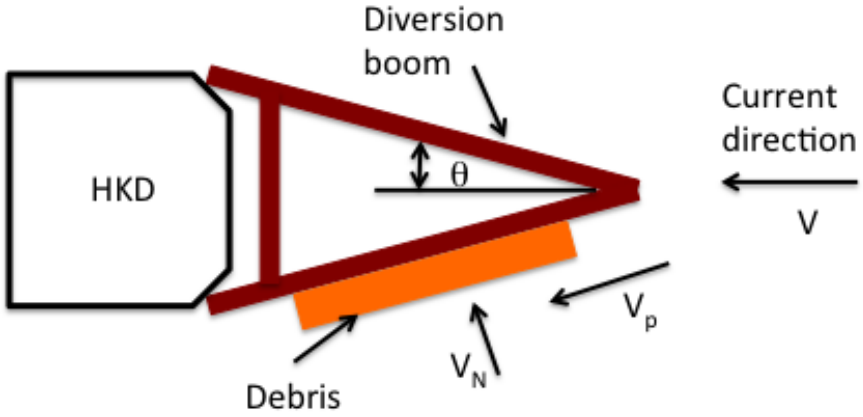

Figure 5. Debris diversion boom upstream from a RISEC device (Johnson et al. 2013).

Generally, diversion systems such as the one shown in Figure 5 are designed in an ad hoc manner with little thought to the factors that might influence the effectiveness of the diversion device to actually divert debris. Intuitively, factors that influence the ability of a diversion boom to divert debris might include friction (μ) between the diversion boom and debris object, the opening angle of the boom (θ), current velocity (V, V_p, V_N), and the sharpness of the front end of the diversion boom. Most diversion booms have a sharp front

end (see Figure 5) that can collect and entrap branches or rough debris edges that catch on the sharp apex of the boom. Because of the force of water, a sharp apex can also penetrate into the surface of woody debris to such an extent that the debris object is held in place, eventually resulting in the collection of significant debris at the front of the diversion boom that can eventually overwhelm it (Pelunis-Messier 2010).

An analysis by Johnson et al. (2013) of the factors affecting debris diversion, following the force diagram shown in Figure 5, addresses the question of when a debris object will slide off of a diversion boom and when it will be pinned. Pinning of a debris object occurs when the component of current velocity parallel to the diversion boom ($V_p = V\cos\theta$) produces a sweeping force that is smaller than the pinning force due to the current velocity normal to the diversion boom ($V_N = V\sin\theta$) and friction between the diversion boom and the debris object. Factors that affect the pinning friction force (F_μ) include friction between the diversion boom and debris, debris object length, θ, and V_N (which is in turn dependent on V and θ).

Sweeping forces that act to push a debris object along the diversion boom surface consist of the force acting on the debris object cross section (log diameter and branches), F_{pE}, and shear force acting on the exposed length of a debris object due to the water flow shear boundary layer between the debris object surface and free flow current of the river, $F_{p\eta}$. The force balance equation to determine if a debris object will be swept clear of the debris boom or be pinned is given by

$$Q = \frac{F_{pE}+F_{p\eta}}{F_\mu} > R \qquad (1)$$

where R is a threshold parameter that determines whether a debris object will be pinned to the diversion boom or swept away, and Q is the ratio of sweeping forces to pinning forces (Johnson et al. 2013).

When Q exceeds R, a debris object will be swept from the debris boom. It is not possible to quantitatively determine the terms in Equation 1; however, since our interest is in the general relationship between performance of the debris diversion boom and the primary parameters that control the pinning and sweeping forces, Equation 1 can be written in a simplified form as

$$Q = \frac{\pi \mathrm{V}\cos\theta\left(\mathrm{V}\cos\theta+\frac{\beta}{2}\right)}{2\mu\beta(\mathrm{V}\sin\theta)^2} > R \qquad (2)$$

where β is the ratio of the debris object length to its cross-sectional area. Figure 6a shows Q as a function of θ for different values of friction (μ) and current velocity. Figure 6b shows $\underline{Q}$ as a function of θ for different β values.

From the results shown in Figure 6, it is apparent that Q is a strong function of θ, which is unsurprising given that the current velocity component parallel to the diversion boom decreases with θ, while the current velocity component normal to the diversion boom increases with θ. As θ increases, the sweeping force decreases while the pinning force increases. Increasing current velocity, reduced friction, and smaller debris length to cross-

sectional area ratio result in increased *Q*. Taken together, the optimal controllable parameters for a debris diversion device are minimized θ and μ.

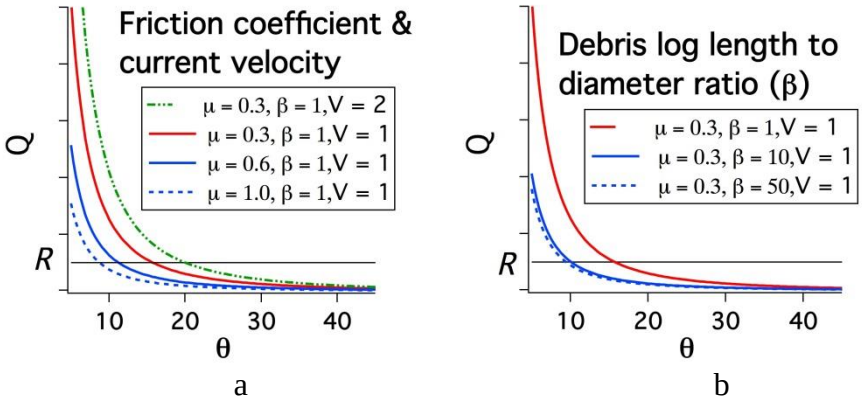

Figure 6. The change in *Q* as a function of diversion boom half-angle (θ) for different μ and current velocity (*V*) (a) and as a function of boom half-angle and debris log length to diameter ratio (β) (b). *R* is arbitrarily selected for illustration (Johnson et al. 2013).

A solution to the problem of debris catching on the sharp front end of a diversion boom is to use a debris sweep (Bradley et al. 2005) that consists of a freely rotating cylinder placed in front of the debris diversion boom's apex point. When impacting the debris sweep, debris can rotate clockwise or counterclockwise (depending on the direction of torque acting on the sweep), allowing diversion of the debris object to the debris boom. Generally, a debris sweep will have asymmetric protrusions on its surface to rotate its cylinder so that small debris objects do not collect in the current velocity dead zone that exists at the front of the debris sweep. The rotating torque produced by the protrusions is quite small, compared with torque forces imposed by large debris objects, and does not restrict the debris sweep cylinder from rotating in either direction to divert such debris objects.

Debris sweeps have proven to be effective at preventing debris collecting on the front of bridges. To prevent damage to a deployed debris sweep, it is important that the sweep be sufficiently robust to withstand forces generated by debris impacts (Tyler 2011). The diameter of a debris sweep cylinder needs to be large enough to prevent branches from a debris object, or root balls, from extending beyond the centerline of the debris diversion boom where debris can catch on the front of the sweep. Determining the optimal diameter for a debris sweep cylinder is not an easy task, as its ability to shed debris with protrusions depends on the perpendicular length ratio of the protruding limb and the opening angle of the diversion boom. Secondary factors that influence the performance of a debris sweep include the debris sweep's inertia and surface friction.

RDDP CAD Design

The RDDP was designed to test the effect of different opening angles and various front-end types that included a debris sweep with hinged vanes to produce rotation, a smooth plastic cover over the hinged vanes to provide a low-friction surface, and a sharp apex angle. A computer-aided drawing (CAD) of the RDDP with a hinged-vanes-equipped debris sweep is

shown in Figure 7. The constructed RDDP is shown in Figure 8a, and the plastic-covered debris sweep and sharp-angled debris diversion front ends are shown in Figure 8b.

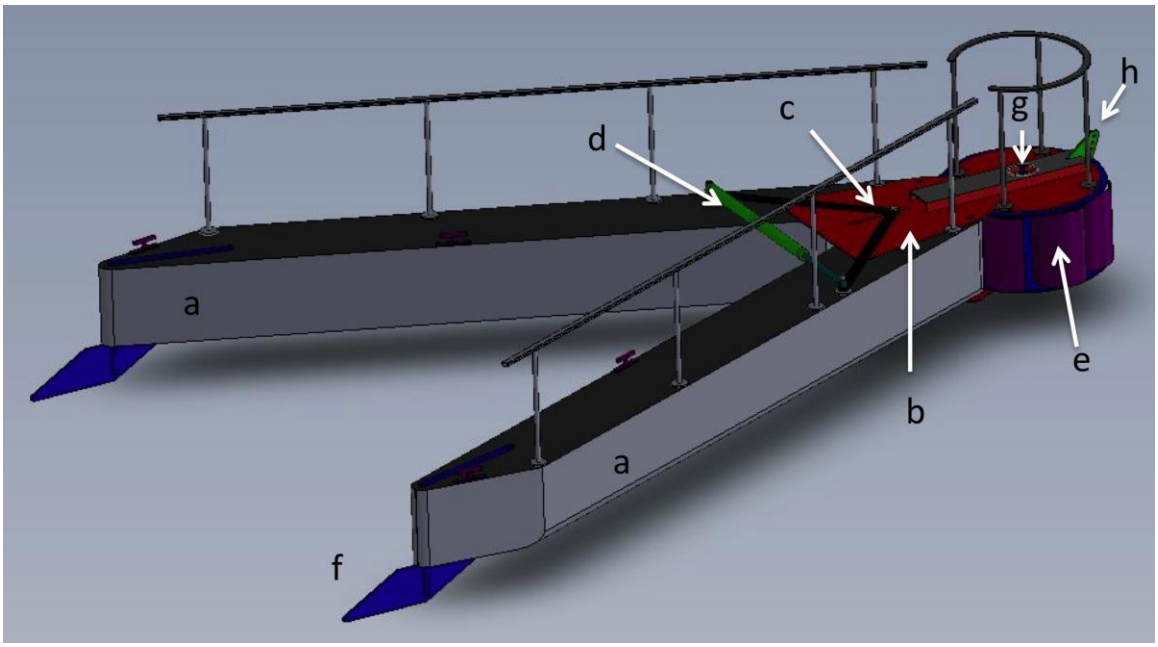

Figure 7. Research debris diversion platform showing the various components including the pontoons (a), the connecting plate between the sweeper and pontoons (b), the reinforcing U-bracket and centering bars (c), the hydraulic ram (d), debris sweep with hinged vanes (e), rudders (f), debris sweep axel head nut (g), and mooring attachment point (h).

a b

Figure 8. RDDP in its closed position showing the debris sweep with hinged vanes (a), and the RDDP front-end mounts shown separately from the plastic-covered V-"nose" 62-degree angled front end and the plastic-covered debris sweep cylinder (b).

Handrails and cleats on the pontoons allow maintenance personnel to tie up a boat and walk around on the RDDP safely. Rails were moved to the inside of the RDDP after preliminary testing indicated that debris limbs could catch on the railing stanchions located on the outside of the pontoons. The curved rail around the front of the RDDP allows workers to brace

themselves when removing debris that might collect on the front of the RDDP or to perform other maintenance tasks on the debris sweep. The opening angle of the RDDP pontoons ranges from 25 to 77 degrees and is set using a hydraulic spreader ram (d in Figure 7).

RDDP Construction

The RDDP consists of two steel pontoons joined in a wedge configuration with the apex of the wedge facing upstream into the river current (Figure 8a, Table 1). A vertical-axis rotating cylinder (1.1 m diameter) is at the leading edge of the wedge. The rotating cylinder employs an array of hinged vanes that exploit the river current to promote rotation. The purpose of the rotating cylinder is to reduce the probability of debris collecting on the leading edge of the RDDP. The angle between the two pontoons of the RDDP is adjustable by means of a hydraulic cylinder, and the rotating cylinder at the leading edge may be replaced with a fixed angled wedge (Figure 8b) in order to compare effectiveness between the two configurations. The pontoons are chambered to allow water ballast to maintain RDDP trim.

Table 1. Nominal RDDP dimensions.

Debris sweep cylinder diameter	1.1 m
Length of diversion pontoons (from center of debris sweep rotation axis	6.1 m
Pontoon width	0.64 m
Pontoon depth	0.64 m
Freeboard	0.18 m

After testing revealed that the hinged vanes on the debris sweep had a tendency to trap debris through a process that was identified as torque balancing (described in the discussion section), the vanes were covered with high-density plastic to reduce friction between the debris sweep and floating debris (Figure 8b).

The opening angle of the pontoons is set using a hydraulic ram-driven system that consists of a reversible hydraulic hand pump (shown on the left pontoon), a hydraulic ram attached to each pontoon (shown lying across the pontoons), and centering bars (Figure 9a). The centering bars, which are attached to a slide pin that rests in a slot cut into the reinforcing U-bracket (Figures 7 and 9a), force the pontoon to open symmetrically about the RDDP centerline.

a b

Figure 9. RDDP centering bars, hydraulic ram, and pump systems (a), and RDDP tethered to the mooring buoy (b).

RDDP Mooring and Testing

RDDP mooring

Moored to the buoy that was connected to an embedment anchor (Appendix A) at the TRTS, the RDDP (Figure 9b) underwent both short-term debris impact testing and long-term deployment testing. The original mooring connection point (Figure 10a) was replaced by a fairlead (Figure 10b) to prevent large-diameter debris objects from catching on the underside of the mooring point. The mooring attachment point for the RDDP was approximately 1.5 m aft of the leading edge of the device, with the mooring line feeding through the fairlead on the leading edge about 0.5 m above the deck of the device. The fairlead ensures that lateral forces imparted by the mooring line are applied at the foremost part of the RDDP to facilitate mooring to the mid channel buoy. Having the mooring attachment point aft of the fairlead allows easy access to the load cells and quick-release device. The quick-release device (Sea Catch model TR8 with a working load rating of 42.6 kN and estimated break strength of 213 kN) allows the RDDP to be released from its mooring line rapidly even when the line is under extreme tension.

a b

Figure 10. RDDP original mooring attachment system with hinged-vane debris sweep (a) and modified attachment system with sharp-angle front end (b).

Figure 11. Mooring buoy (1.2 m diameter by 1.9 m length cylinder with a 1.9 m length conical section on the anchor chain end) with RDDP mooring line on its bitt.

The RDDP was pushed into position by a motorized tender and attached to the mooring buoy (Figure 11) by a synthetic mooring line with an eye at the end that was placed over a bitt on the buoy. The buoy was located in mid-channel connected to a heavy chain and 1360 kg embedment anchor.

The RDDP and buoy connection together constitute a debris diversion system where the buoy acts to intercept large debris items. Due to the buoy's large buoyancy and conical front end, large debris objects tend to ride up the buoy and eventually

slide off or break, as the debris mass is generally not sufficient to submerge the buoy. The anchor and chain from the riverbed to the buoy are rated at 205 kN, which should withstand most debris impacts. Debris masses observed on the Tanana River, albeit infrequently, could overwhelm the buoy-RDDP system; hence, precautions should be taken to protect infrastructure from them. For example, a look-ahead video system with an automated warning alert and a quick-release mechanism that is load cell based may provide the ability to remove infrastructure prior to debris impact or to recover infrastructure as it moves downstream.

Data Acquisition and Sensors

The data acquisition system used for the RDDP was a Campbell CR1000 data logger that records analog signals from the load cells. The logger operated on power supplied by a 12 V battery. The logger supplied a 2.5 VDC excitation for HRS-2K (2000 lb) and HRS-20K (20,000 lb) load cells supplied by Load Cell Central (Figure 12). The CR1000 data logger and battery were placed in a small waterproof Pelican case and lashed to the deck of the RDDP.

Campbell Scientific PC200W PC support software was used to communicate with the data logger, and the logger programs were created using the Campbell Shortcut program. Two programs were used during deployment. When the RDDP was to be deployed unattended for a number of days, samples were taken at 1-second intervals with average minimum and maximum loads recorded at 60-second intervals. When the RDDP was attended, the logger recorded each 1-second sample along with its corresponding time.

During debris testing, GoPro video cameras were mounted on the RDDP on a mast (approximately 2.5 m tall) near the forward end of the port pontoon (Figure 12). The cameras recorded activity forward and aft of the RDDP. The cameras could operate continuously for about 4 hours, at which time the camera batteries and memory cards would be replaced. Additionally, a chase boat recorded debris impact tests using a video recording system.

RDDP/Buoy Performance Tests

The primary goals of the RDDP buoy tests were to determine (1) how robust the RDDP was to debris impact forces; (2) how easily the RDDP shed debris using different RDDP front ends and opening angles; (3) the distance behind the RDDP that remained debris-free after debris was diverted; and (4) the amount of turbulence created by the RDDP that might affect the performance of a RISEC device installed behind the RDDP. To test the robustness of the buoy and RDDP system to survive debris impact forces and divert debris, a series of direct impact tests were conducted on the buoy and the RDDP separately along with long-term unattended deployment testing.

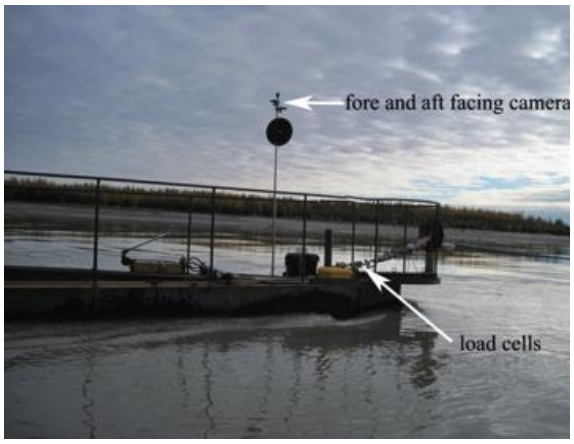

Figure 12. RDDP photo showing the position of GoPro cameras and load cells.

Direct impact tests involved harvesting large debris objects from an eddy located upstream from the buoy/RDDP system. The debris objects were maneuvered to impact the buoy or RDDP perpendicular to the current flow direction and at the center of the debris object's length (Figure 13). Such testing provided the maximum impact forces on both the buoy and RDDP and the most difficult conditions for clearing debris, since the forces of the river current were equally distributed along the debris object's length about the RDDP and buoy centerline.

Figure 13. Direct debris impact test of the RDDP using a log perpendicular to the current flow direction. Debris object just before impact (a), on impact (b), sliding off the debris sweep (c), and clearing the RDDP (d).

Direct impact tests were done using a variety of tree sizes, shapes, and types for RDDP opening angles that ranged from 25 to 77 degrees and RDDP front-end attachments (Figure 8). Once tests demonstrated that the RDDP could survive major debris impacts, the diversion device was left moored to the buoy for extended periods during the summers of 2011 and 2012.

River Hydraulic Measurements

During August 2012, multiple cross-river ADCP sections were performed to measure current velocities (Figure 14) at cross-river sections spaced 20 m apart, beginning above AHERC's buoy and ending downstream of the RDDP. Three different sets of measurements were conducted to analyze the RDDP influence on river current flow velocities: no RDDP deployed in the river, RDDP deployed with maximum opening configuration, and RDDP deployed with closed configuration, that is, the minimum opening.

Derived variables from these measurements in the Cartesian coordinate system include total river discharge, the potential force of the water on an object fixed in-stream (Figure 15), and velocity fluctuations as a proxy for turbulence (Figure 16). Velocity fluctuations were calculated by partitioning the velocity cross-sections into quadrilateral blocks of ~2.25 m^2, an area chosen as representative of the turbine cross-sectional area exposed to river flow. Velocity fluctuations, u', for each bin in each block in the cross-sectional, along-channel, and

vertical directions were calculated using $u' = u - \bar{u}$, where $\bar{u}$ denotes the average velocity, and u denotes the individual bin velocity.

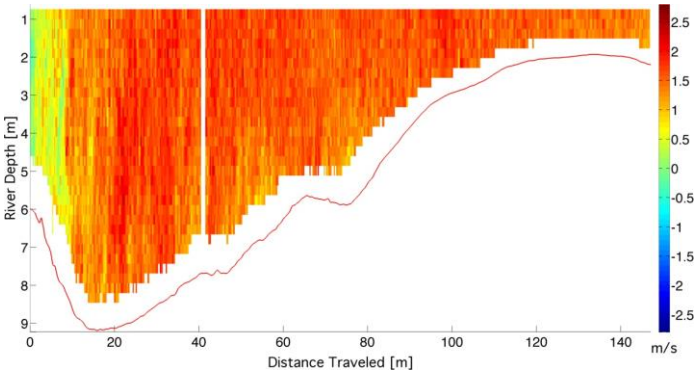

Figure 14. North velocities (m/s).

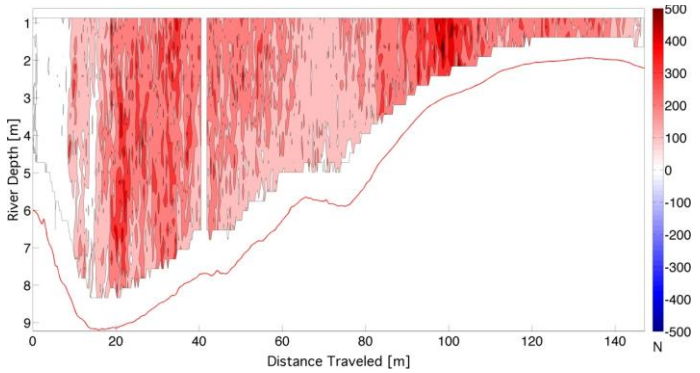

Figure 15. Potential force (N) or rate of momentum change created by the water on a fixed object in the north direction.

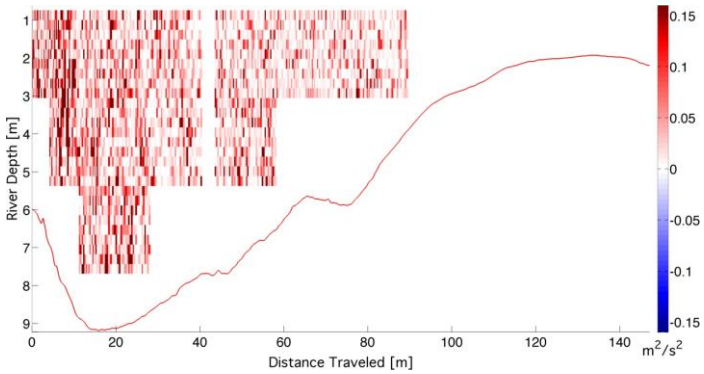

Figure 16. Velocity fluctuations (m^2/s^2) in the north direction.

Alternate processing methods of the measurements are being developed, where the velocity measurements are first rotated into along-channel and cross-sectional velocities, then projected into an ideal straight transect, and finally interpolated over a uniform grid.

River Debris Time-lapse Photography

A solar/battery-powered time-lapse video debris observation system (VDOS) was developed and installed onshore at the TRTS to observe floating debris (Figure 17). A computer system controls the mounted cameras and the storage of recorded pictures. The specifications for the cameras and computer systems are as follows:

- Processing: Dell Vostro 1014 laptop
- OS: Windows 7 Home Premium
- Image archive program: Matlab
- Video camera: Two FaceVsion TouchCam L2 cameras with 2-megapixel resolution mounted in modified Pelican Micro Case dry box with clear cover.

Appendix B provides the specifications for the independent power box supply.

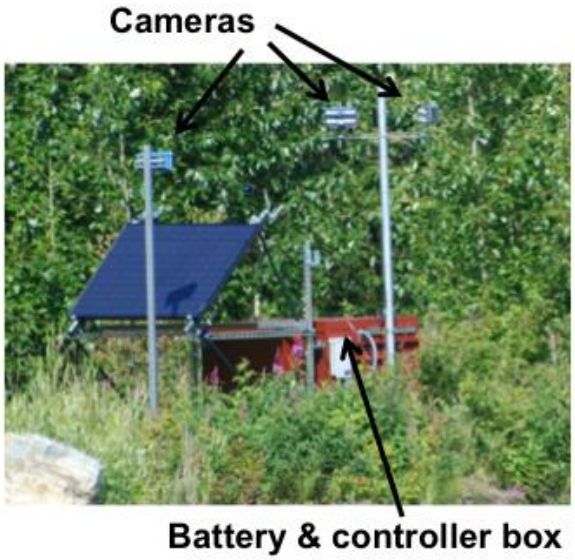

Figure 17. Video debris observation system. The system is mounted onshore with cameras pointed at the RDDP/buoy location and upstream from the RDDP/buoy. A third (security) camera is pointed back at the system. This picture was taken from a boat tethered to the buoy looking back at shore.

The edge detection method was tested to identify debris in the recorded images as a first step to automating interpretation of video images of debris. One of the most important properties of an object is its physical edge, which correlates with object boundaries, changes of surface orientation, or material properties. The objective of the edge detection technique is to characterize changes in intensity of an image in relation to the physical processes that originated them. The edge detection method is composed of two steps: a regularizing filtering operation step and a numerical differentiation step (Torre and Poggio 1986).

The following are examples of other methods used in object recognition:

- Corner detection: Corners are image points that display a strong two-dimensional intensity change that may be matched between images (Trajković and Hedley 1998).

- Blob detection: A blob is a compact region lighter or darker than its background, enclosed by a smoothly curved edge (Danker and Rosenfeld 1981).
- Ridge detection: A ridge on a surface is defined by means of extrema of curvatures along lines that are intersection curves of the surface with a plane (Lang et al. 1997).

Results

RDDP Direct Debris Impact Testing

Direct debris impact tests conducted on the RDDP are summarized in Table 2, and video documentation of tests are archived at the Alaska Center for Energy and Power YouTube Channel (ACEP 2014a, 2014b, 2014c, 2014d, 2014e, 2014f, 2014g, 2014h). Initial tests were done on the mooring buoy and the RDDP with a hinged-vane debris sweep front end (Figure 8a). Sizable trees of various cross sections up to 0.7 m and lengths up to 20 m were retrieved from a nearby eddy and pulled into the current for it to push them perpendicular into the buoy or RDDP. Tree types included spruce with extensive branches and needles, logs stripped of bark and limbs, and twisted birch. Numerous small-diameter debris objects were used to help examine the influence of debris mass on RDDP performance.

Table 2. Debris introduction tests.

Date	Forward configuration	Pontoon angle (degrees)	Debris type	Remarks
8/24/2012	Debris sweep with plastic	77	Standard log	Hung up on debris sweep and end of pontoon (i.e., debris was pinned to pontoon)
8/24/2012	Debris sweep with plastic	58	Standard log	Debris shed easily
9/6/2012	Fixed V-"nose"	58	Standard log	Debris log "t-boned" and slid off to starboard
9/6/2012	Fixed V-"nose"	58	"Branchy" log	Debris log "t-boned" and hung up on nose; required clearing assistance with boat
9/6/2012	Fixed V-"nose"	58	Standard log	Debris rolled under starboard side
9/6/2012	Fixed V-"nose"	58	"Branchy" log	Off-center strike; branches hung up on rail stanchion
9/6/2012	Fixed V-"nose"	77	18 m log	Debris log "t-boned" and rolled under RDDP
9/6/2012	Fixed V-"nose"	77	Brush	Repeated test twice; rolled under RDDP
9/6/2012	Fixed V-"nose"	77	Brush	Debris struck nose, but did not hang up
9/6/2012	Fixed V-"nose"	25	Brush	Debris broke up and shed
9/6/2012	Fixed V-"nose"	25	Brush	Two events where brushy debris hung up
9/6/2012	Fixed V-"nose"	25	Brush	One event where brushy debris was shed by V-angle nose

Mooring Buoy Direct Debris Impact Tests and Performance Characteristics

Impact tests on the buoy (Figure 18), which occurred early in the testing phase, were not documented with video. These tests involved pulling debris objects to a position in the river, their long axis perpendicular to the flow. The debris objects were released such that impact with the buoy would occur near the middle of the debris object's length. Generally, large

debris objects would ride up the face of the buoy and eventually slide off the buoy to one side or the other, depending on the direction of torque acting around the point of contact caused by the current velocity. The process of debris shedding by the buoy caused most debris objects to reorient themselves such that the long axis of the debris was parallel to the current velocity. This reorientation effect made it more likely that any subsequent impact with the RDDP would be end-on, which is much easier to clear than impacts that occur with debris oriented perpendicular to the current direction.

Figure 18. Mooring buoy.

Some large debris objects would remain pinned temporarily to the buoy after impact before sliding off the buoy surface. In these cases, the friction between the debris object and the buoy prevented (or made it difficult) for the debris object to slide along the surface. As a result, debris would rock back and forth under the influence of river current turbulence that caused the torque maximum to shift back and forth across the debris contact point with the buoy. Because the buoy was also being pushed around by current turbulence, the contact between a debris object and buoy was unstable, meaning that the debris object eventually slid (or hopped) along the buoy surface until consistent maximum torque caused the debris object to slide off the buoy. During one test, an exceptionally large spruce tree of about 0.7 m base diameter and 20 m length caught on the buoy, and the force of the current bent it around the buoy and eventually broke the tree at the point of contact with the buoy.

Small debris often did not contact the buoy because the wake created by the buoy pushed debris away. This wake effect has been suggested as a method to divert debris by using the momentum of the wake to redirect a debris object. Observations from our tests indicate that the ability of buoy wake to redirect debris is limited to smaller debris, as a considerable mass of debris has sufficient momentum to move through the wake with little effect.

By design, only a single anchor chain runs between the riverbed and the mooring buoy to limit the interception cross section to subsurface and surface debris in the river, which proved to be a significant problem for the surface-deployed New Energy turbine at Eagle. The mooring line between the buoy and the RDDP ran parallel to the water surface with the expectation that a RISEC device moored behind the RDDP would also have a mooring system with lines running parallel to the water surface. This system of attachment is effective at reducing the amount of subsurface debris that accumulates on the anchor chain, because the mooring buoy is free to move around due to the river's turbulent current. The mooring line to the RDDP remains free from debris because it runs on the river surface parallel to the flow direction. During our two-year testing program, only two events of debris intercepting

and riding up the anchor chain to the front of the buoy were observed, and these were easily removed.

In addition to reducing the interception cross section, the single anchor chain connection to the mooring buoy could be used to protect an electrical cable running from a RISEC device on a floating platform to the riverbed and then to shore. During the Eagle tests, subsurface debris caught on the power cable that ran from the pontoon barge vertically to the riverbed, requiring that the cable be cut when the debris could not be removed. Running a power cable down the anchor chain allows the load exerted by any debris to be taken up by the chain rather than the power cable and provides the possibility that debris will ride up the chain, where it will be dislodged by the motion of the buoy or can be readily removed (since the chain will be slanted at an angle downstream from the anchor point). In situations where the primary mooring buoy is too far ahead of the RISEC device to feasibly run a power cable parallel to the anchor chain, a second buoy and anchor point could be placed immediately in front of (or behind) the RISEC device specifically to protect a power cable after its deployment.

RDDP Direct Debris Impact Tests, Long-term Deployment and Performance Characteristics

Direct debris impact tests were conducted on the RDDP with different opening angles and different front end configurations (Table 2). In these tests, logs were towed to a position just downstream from the mooring buoy and released to impact the front end of the RDDP (Figure 13).

The first series of tests were done using the debris sweep front end with hinged vanes. While the debris sweep with hinged vanes caused some debris to rotate off the sweep onto the RDDP pontoons, there were also events where debris objects impacted the debris sweep and remained pinned to it, oscillating but not rolling off to one side or the other (Figure 19). Close review of video recordings indicate that the debris sweep was free to rotate, but only oscillated, even when the log canted at a sharp angle to the RDDP centerline. Force analysis of possible causes of the observed debris pinning events on the debris sweep with hinged vanes indicates that three factors contribute to debris pinning:

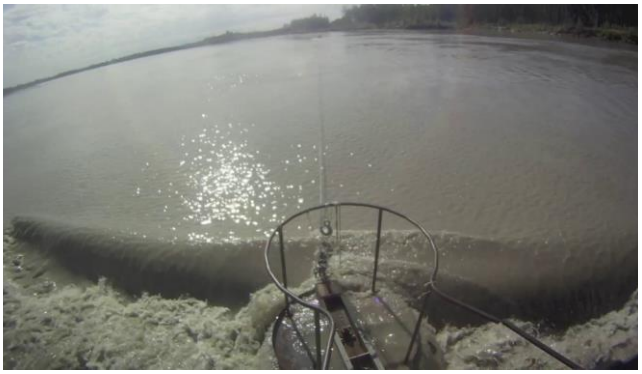

Figure 19. Debris object torque balanced on the RDDP's debris sweep with hinged vanes.

1. The edges of the hinged vanes dig into debris, creating a fixed contact point between the debris sweep surface and the debris objects and requiring that the debris sweep rotate far enough for the vanes to release from the debris before it will clear the debris sweep.
2. The debris sweep inertia is considerable due to its being built to withstand significant impact loads. The torque imbalance in a rotational direction (clockwise or

counterclockwise) must last long enough to overcome debris sweep inertia and rotate the sweep far enough to release the hinged vanes from the debris.

3. River turbulence is variable, such that torque imbalance caused by current forces acting on pinned debris appears to reverse the torque direction too quickly for the debris sweep to rotate far enough to release the debris from the hinged vane. As a result, debris can become stably balanced on the sweep (torque balanced). An example of a torque-balanced log is shown in Figure 19 and at http://youtu.be/2Z-l_efgwZA (ACEP 2014h).

To overcome the torque balance problem caused by the debris sweep's hinged vanes, the debris sweep was covered with a high-density low-friction plastic (Figure 8b). This cover provided a low-friction surface that allows debris to slide along the surface of the debris sweep when river current velocity produces torque imbalance, without having to overcome the debris sweep's inertia. Observations indicate that when a debris object impacts the RDDP debris sweep near the debris balance point, the current-produced torque imbalance initially causes the debris object to slide along the debris sweep's surface. As the debris object continues sliding, the debris sweep starts turning in the direction of the torque imbalance. The combined effect of debris sweep rotation and debris sliding along the surface of the debris sweep's plastic cover effectively clears the debris (ACEP 2014i; http://youtu.be/W-WFmLVPHzE). Since the plastic covering was installed, no debris has pinned against the debris sweep surface during two years of long-term deployment.

A series of direct impact tests were performed on the RDDP with the sharp-angled front end (Table 2, fixed V-"nose") to examine its ability to shed debris compared with the debris sweep. The sharp-angled front end did shed debris, but had many more incidents of debris hanging up (Figure 20) and debris rolling under the RDDP than the debris sweep. This, taken with the experiences of debris buildup using the sharp-angled front end during the RISEC device demonstrations at Ruby and Eagle, Alaska, indicates that the debris sweep is much more effective at preventing debris from hanging up at the front of the RDDP than the sharp-angled front end is.

Figure 20. Debris object impinged against the sharp-angled RDDP front end, 62-degree angle.

RDDP Debris Impact Loads

A load cell and data logger data acquisition system was used to monitor the frequency and magnitude of forces imposed on the RDDP. Over the course of the 2012 summer season, between late June and mid-September, the load cell logger recorded twenty-eight days of load information. During the periods of active monitoring, the overall load on the RDDP varied with the river stage, which can be a surrogate for river velocity, with forces from debris impacts superimposed on the hydrodynamic drag (Figure 21). Drag force magnitudes are correlated nonlinearly with river stage, because the power generated by current flow is related to the cube of the river current velocity (Figure 22)

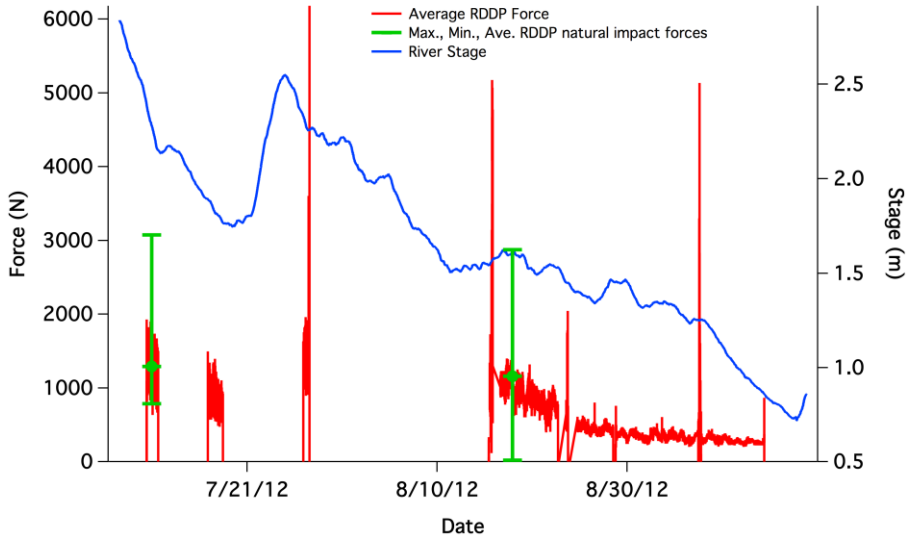

Figure 21. RDDP drag and debris impact force and river stage as a function of date.

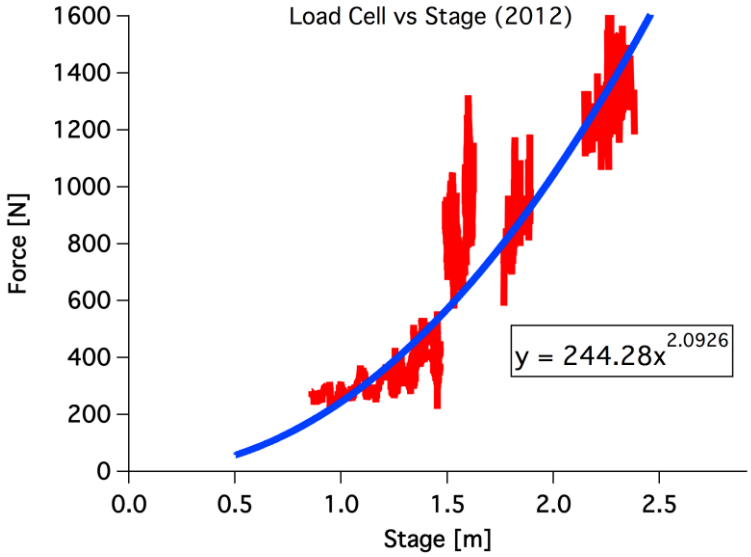

Figure 22. RDDP force as a function of river stage.

A number of debris tests were performed during the 2012 season to explore the nature of interaction with the RDDP. On August 24, 2012, a series of tests were performed to qualitatively note the behavior of debris. A straight, branchless aspen "standard log" was selected as the test debris. After impact, the log was towed back upstream and reintroduced. The dimensions of the standard log are given in Table 3.

Table 3. Dimension of the standard log using in direct debris impact tests.

Length	Butt diameter	Mid diameter	End diameter
12.3 m (40.5 ft)	0.23 m (9 in.)	0.22 m (8.7 in.)	0.12 m (4.7 in.)

Forces from the impact of this log are noted as short-term spikes in Figure 23. The longer-term variations of the load on the RDDP between 3:30 P.M. and 4:15 P.M. are a result of changing the angle of the RDDP pontoons, which increased the drag forces on the RDDP from the river current.

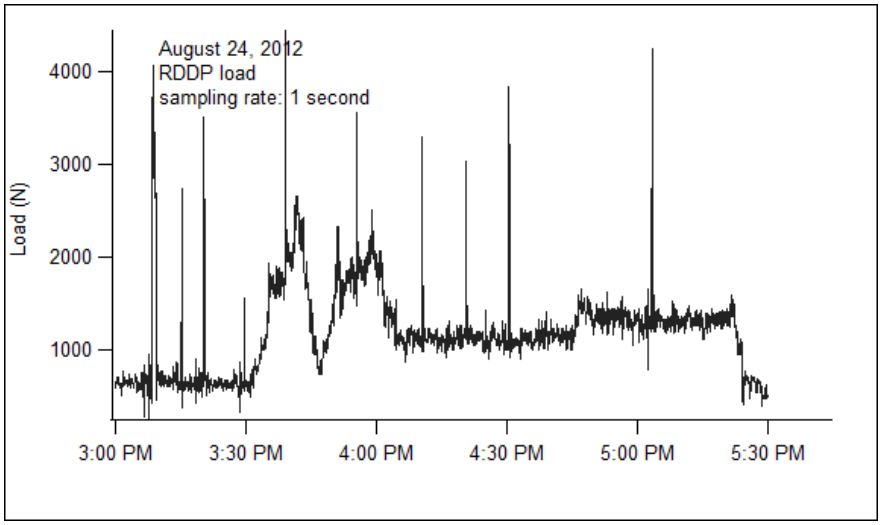

Figure 23. Force history of debris direct impact tests from a standard debris log (Table 2).

At 3:20 P.M., the log was well centered when it struck the RDDP and remained in equilibrium for approximately 15 seconds before starting a slow shedding process. The reduction in force in the following seconds suggests a smaller cross section of the log being exposed to current as the angle of the log changes. The force resulting from the impact and the slow reduction of force during shedding are presented in Figure 24. The data from August 24 were recorded at a sampling rate of 1 second.

During the twenty-eight days of data collection, the RDDP was unattended on two instances when short-term loads increased to more than double the average load. The data suggest a short-term impact because of the single high maximum load and a minimum much lower than the average load. The minimum load is instructive because during an impact the work done is that of the mooring system chain catenary straightening and the mooring line stretching. After the impact load diminishes, the energy added to the mooring system moves the RDDP and mooring buoy farther upstream than its normal position, which is then

followed by a period of reduced load on the mooring line as the system returns to equilibrium.

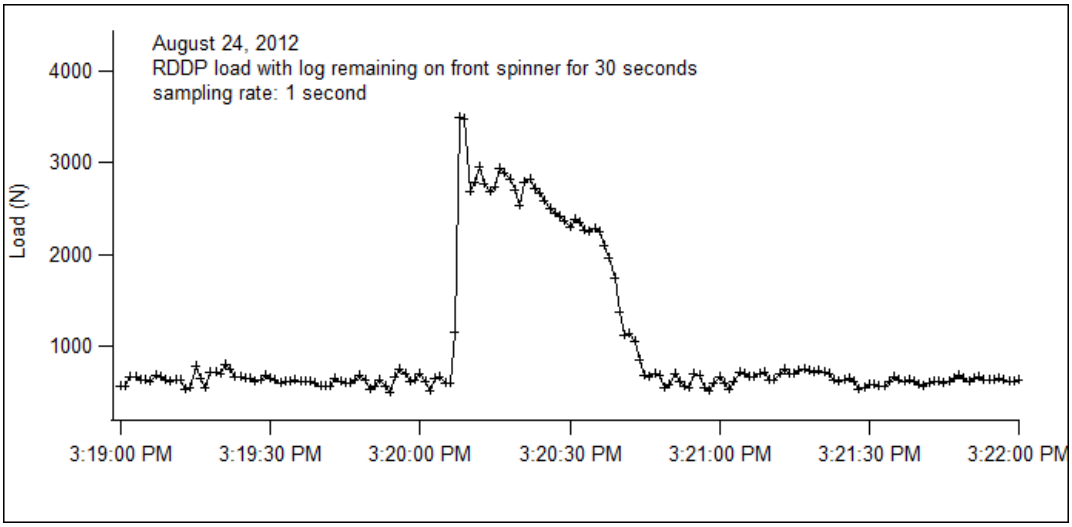

Figure 24. Force history of a direct debris impact from the time of impact until it clears the RDDP.

An example of the load variation as the RDDP returns to equilibrium is illustrated by Figure 25, which shows 5 minutes of data recorded at 1-second intervals on September 6, 2012. In this event, a log introduced into the current upstream of the RDDP resulted in a perfect 90-degree impact.

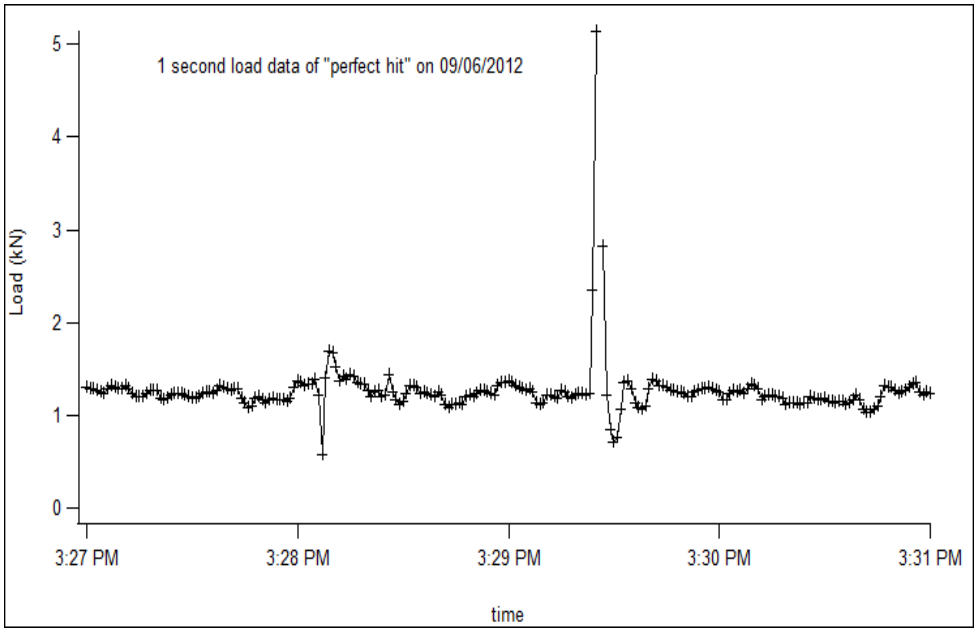

Figure 25. One-second impact force data for a 5-minute period of short-term impact.

The force data for the two short-term debris impacts while the RDDP was deployed long-term and unattended are presented in Table 4. The loads recorded over the entire season are presented in Figure 21. The load spikes displayed in Figure 21, other than those of July 10,

2012, and August 17, 2012, were a result of intentional debris introduction or manipulation of the RDDP. Long-term deployment data were sampled at 1-second intervals, and the maximum, minimum, and average force values were stored every minute (Table 4). Additional memory recently acquired for the data acquisition system allows storage of data at a rate of less than 1 second to improve the analysis of the load data.

Table 4. Load cell data for debris impacts on the unattended RDDP during long-term deployment. Data sample rate 1/second over a 60-second recording interval.

Date	Average Force (N)	Maximum Force (N)	Minimum Force (N)
7/10/12 22:43	1291	3074	787
8/17/12 22:18	1160	2873	19

The maximum load of 6000 N plotted in Figure 21 took place on July 27, 2012, at 1:19 P.M. and was the result of a log intentionally positioned to impact the RDDP. The load parted the sacrificial link designed to protect the HRS-2k load cell from load beyond its design capacity. A higher capacity load cell, HRS-20k, was added to the system in August 2012 to accommodate larger loads, but no excessive loads were experienced for the rest of the season.

Debris Clearing Characteristics of the RDDP Pontoons

Analysis of the debris clearing efficiency of a diversion boom, given by Equation 2 and shown in Figure 6, indicates that friction between debris and the RDDP pontoon surfaces and the opening angle of the pontoons are the primary factors controlling how well the RDDP sheds debris. As the pontoon opening angle increases, the forces pushing debris objects against the RDDP pontoons increase relative to forces acting to cause debris objects to slide along the RDDP pontoon surfaces. This situation results in the RDDP's decreased ability to divert debris through the process of debris pinning against the pontoons, increased debris residence time on the RDDP, and higher undertow forces acting on debris objects.

Tests conducted to examine the effect of the RDDP opening angle confirmed that as the RDDP opening angle increased, the ability of the RDDP to shed debris decreased. The RDDP pontoons shed debris up to opening angles of about 58 degrees, beyond which debris becomes pinned against the pontoons (Table 2, Figure 26). Pinning occurred primarily when debris caught on small protrusions extending from the pontoons, such as weld beads and sharp angles, and the rough surface of the pontoon's steel surface. Debris pinning also occurs when branches from a debris object catch on protrusions from the RDDP, such as the stanchions of the guardrail installed for personnel safety on the pontoons (Figure 27).

Figure 26. Debris object pinned to the RDDP pontoon, with a pontoon opening angle of greater than 75 degrees.

Figure 27. Debris object caught on a stanchion of the RDDP guardrail.

Increasing the pontoon opening angle results in increased residence time for debris objects on pontoon surfaces before the debris clears the RDDP. Increased debris residence time against a pontoon can cause a debris object to start counter-rotating (i.e., rotating counterclockwise when viewed from the river's right bank) due to water flowing underneath the debris. Debris counter-rotation can result in the debris object rotating under the RDDP pontoon rather than being diverted by sliding along the pontoon. Rotation under the RDDP pontoon is most noticeable when debris objects are twisted and act like a corkscrew or when debris objects have an extensive branch network that provides added drag when under water, extending below the bottom of pontoon surfaces. As twisted debris objects counter-rotate, one end of the debris object can be depressed below the pontoon bottom, allowing the rest of the debris object to spiral under the pontoon (Figure 28)

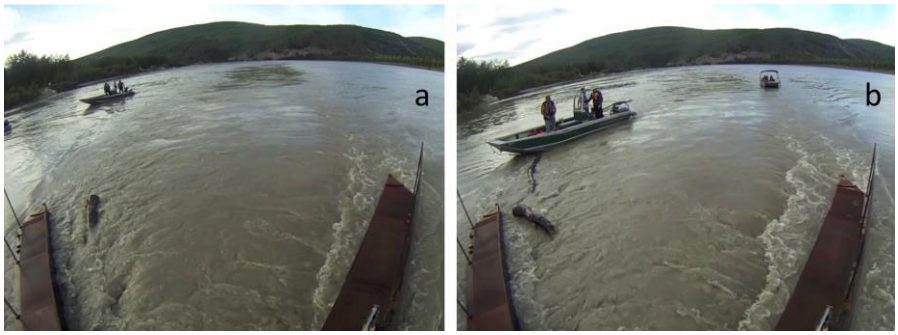

Figure 28. Twisted debris object rotating under the RDDP.

Flow Path Characteristics of Diverted Debris

Once deflected, debris tends to remain clear of the river current flow path immediately behind the RDDP (Figure 29). Two processes help to prevent debris from back filling into the current flow path behind the RDDP. The first process is that debris is moved from its

original flow path to a new flow path outside the edge of the RDDP. The new flow path line is generally parallel to the flow path lines behind the RDDP, such that there is little direct force to move a debris object into the region behind the RDDP.

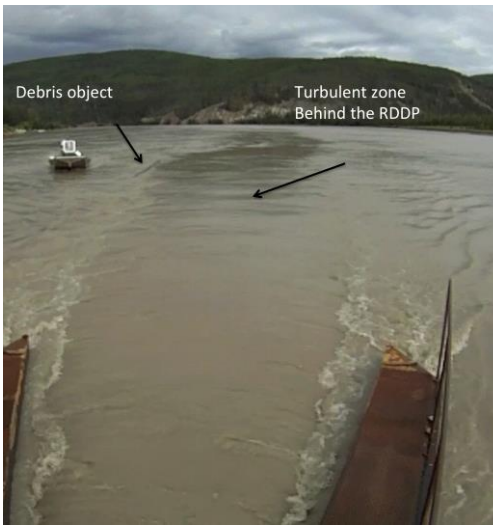

Figure 29. Flow path wake behind the RDDP with diverted debris object along its left hand edge.

River turbulence and changes in the overall direction of the river flow can exert forces to move debris objects into or away from their new flow path lines. However, these effects are relatively small in straight river sections, such as exist at our mooring buoy site. A second process at work that helps to prevent debris from moving in behind the RDDP is an upwelling of water that occurs immediately behind the RDDP debris sweep and that creates a slight outflow away from the centerline of the RDDP (Figure 29). The outflow of water away from the RDDP centerline counteracts forces tending to push debris into the current flow path behind the RDDP.

Debris can move into the current flow path behind the RDDP if debris rolls under the RDDP or when small (low inertia) debris is pulled behind the RDDP by vortex swirls created at the rear edge of the diversion pontoons. Small protrusions on the RDDP pontoons can create a moment arm on longer debris objects causing them to rotate into the current flow path behind the RDDP. In addition, substantial inertia debris objects can cause the RDDP to rotate around its front mooring attachment point such that the debris object is not completely diverted from its original path. The extent of debris diversion that occurs in this situation depends on the relative momentum of the debris object compared with the inertia of the RDDP.

Hydraulic Measurement Results

A preliminary examination of the river current flow field and turbulence in the wake of the RDDP was conducted to determine the effects of the RDDP on the available kinetic energy behind it. In a preliminary write-up, Toniolo (2013) concluded that cross-river ADCP transects were unable to detect changes in the river current due to the introduction of the RDDP. The natural and considerable variability of the river flow masked any signal of the RDDP's wake in such transects. In contrast, using a similar qualitative analysis, Toniolo concluded that quasi-stationary ADCP measurements (Figure 30) were able to detect a decrease in the northward directed near-surface velocities (Figure 31) as well as an increase in the westward directed near-surface velocities in the RDDP's wake. These changes were attributed to the presence of the RDDP. Changes in river flow direction were negligible several meters distant from the RDDP. These conclusions are preliminary and are qualitative characterizations of the effects of the RDDP on the river flow field.

Figure 30. Quasi-stationary velocity measurement locations around the RDDP. Flow direction is from right to left (Toniolo 2013).

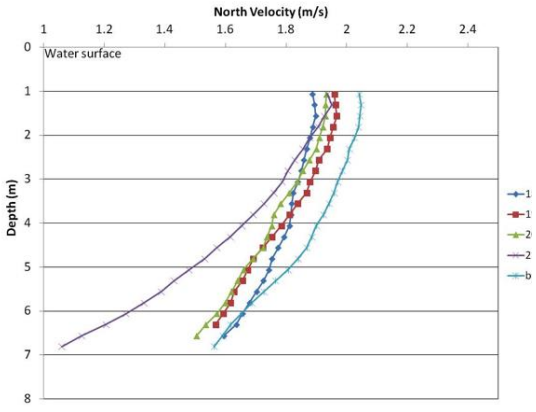

Figure 31. Average velocity in the north direction at different measurement locations (Toniolo 2013).

Shore-Mounted Time-Lapse Camera Results

Applying an edge detection technique to camera images produces processed pictures that highlight the moving debris from the background. In Figure 32, a composition of four pictures is shown, where the floating log is seen as a bright white line segment over the gray background (water surface), moving progressively downstream. The contrast difference between the line segment and the background as well as the movement of the line segments may provide a way to automate surface debris detection to provide statistics about the frequency, size, timing, and type of debris in the river.

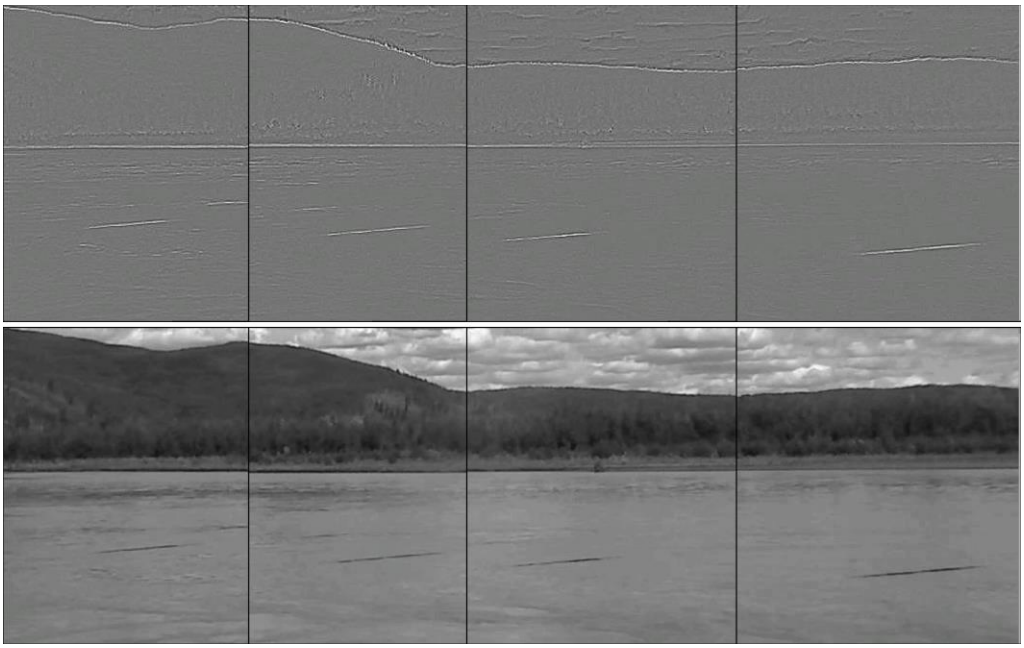

Figure 32. Composition of four pictures highlighting the moving debris from the background (top) after applying the edge detection method. The original images are placed in the bottom.

Discussion of RDDP Effectiveness and Implications for Improved Performance of Diverting Surface Debris

RDDP System Design Purpose and Limitations

Experiences from deploying a surface-mounted RISEC device at Eagle demonstrated that debris can collect on anchor cables leading to the floating platform supporting the RISEC device and on electrical cables extending into the water, as well as in front of the floating platform. Debris impacts also have the potential to damage the RISEC infrastructure. The RDDP system (RDDP, mooring buoy, embedment anchor) was constructed to limit the number of cables running from the river surface to the riverbed and to withstand both large inertia and small inertia impacts from a variety of debris types. While the effectiveness of the RDDP at diverting debris was examined for many debris types, it was not possible to test debris objects with big root balls or debris objects that travel downriver in a vertical orientation with the root ball either suspended in the water or scraping along the riverbed (Figure 33).

a b

Figure 33. Debris object with root ball (photo: Jack Schmid) (a) and upright debris object scraping the river bottom (just ahead of and on the right-hand side of the RDDP) (b).

RDDP System Performance

In general, the RDDP system performed well at withstanding the forces of debris impacts and diverting debris from the river current flow paths behind the RDDP. The single embedment anchor connected to a mooring buoy usually did not collect debris on its anchor chain and withstood significant debris impacts. Two small debris objects did ride up the anchor chain, but they were easily removed. The lack of debris collecting in front of the buoy is attributed to its continuous movement in the current, creating an unstable surface for debris to contact. In addition, the conical shape and large buoyancy of the mooring buoy forced debris to slide off the buoy, often reorienting the debris parallel to the current flow, or to break apart. Tangled debris can break apart on impact, and in one case, a large tree broke into two smaller lengths.

Debris that managed to get by the buoy and impact the RDDP did not tangle in the tether line extending from the buoy to the RDDP. For the most part, such debris was effectively diverted by the RDDP using a cylindrical debris sweep and pontoon opening angles of less

than 58 degrees. There were limitations, however, to the RDDP's effectiveness at diverting surface debris, including situations such as:

1. Debris hanging up on the front of the debris sweep when it was installed with hinged vanes when debris impacts the debris sweep in an orientation perpendicular to the current flow and at the middle of the debris object: The hinged vanes dug into debris objects, holding them in a balanced condition, because the river current did not create enough continuous torque (due to turbulence-induced torque variations) to overcome the debris sweep inertia to rotate the debris object out of the way. This problem was solved by covering the hinged vanes with a smooth plastic surface that allowed debris objects to slide along the surface of the debris sweep. Once the torque magnitude was sufficient to overcome debris sweep inertia, the debris sweep rotated to move the debris to the pontoon surface.
2. Debris hanging up against the apex of the angled RDDP front end, which demonstrated that angled front ends are not effective at clearing debris: The sharp angle can dig into woody debris to hold it in place, or branches from debris objects can catch at the apex of the device. These problems do not appear to be improved much by covering the surface with plastic.
3. Debris pinning against pontoons with wide opening angles—pontoon opening angles greater than 58 degrees: At wider opening angles, the force pushing the debris against the pontoon created resistance to sliding that was greater than the current force needed to slide the debris along the pontoon surface. The source of sliding resistance was pontoon surface friction and protrusions from pontoons (e.g., weld beads).
4. Twisted debris or debris with extensive branches being swept under the RDDP pontoons by the river current undertow: Twisted trees can corkscrew under the bottom of a pontoon as it rotates counterclockwise with respect to the right bank of the river. Branch networks that extend to depths below the bottom of a pontoon can create a strong undertow that pulls debris under the pontoon.
5. Large inertia debris with sufficient momentum that cause the RDDP to rotate around its tether anchor point and prevent a debris object from being fully diverted from the protected flow paths behind the RDDP: The extent of RDDP rotation and debris diversion depends on RDDP inertia and debris momentum.
6. Debris hanging up on pontoons when branches catch on protrusions, such as the stanchions of the safety guardrails.

Recommendations for Improving RDDP System Performance

To improve RDDP performance and reduce the probability of debris entering the protected flow paths behind the RDDP, we suggest the following changes to the RDDP system:

1. Increase buoyancy and modify the shape of the buoy nose so that it is more hydrodynamic to reduce generated river turbulence.
2. Remove the hinged vanes on the debris sweep to reduce its inertia and install a smooth, low-friction, hard plastic surface to allow debris to slide along the debris sweep surface until the developed torque can rotate the debris sweep.

3. Install a smooth, low-friction hard plastic covering on the surfaces of the RDDP pontoon and the debris sweep vanes to reduce the sliding resistance of debris.
4. Operate the RDDP with a debris opening angle only as wide as needed for protecting a RISEC device installed behind it to reduce the forces pushing debris against the RDDP pontoons and increase the debris-clearing forces. This opening angle will reduce the probability of debris objects being swept under the RDDP pontoons by river current undertow.
5. Connect the RDDP to any RISEC floating platform located behind it such that the inertia of the RISEC platform counteracts rotation of the RDDP about its tether anchor point. Doing so provides additional inertia to counteract the effect of impacts from large inertia debris objects to push past the RDDP by causing it to rotate out of the way.

Conclusions

Surface and subsurface debris in Alaskan rivers pose a serious hazard to the deployment of RISEC devices. Most debris floats at the water surface, but debris can be carried by current at any location through a river's depth. Some debris objects extend from the riverbed to the river surface. When deployed and operated from floating platforms, RISEC devices are susceptible to floating debris impacts that can clog the front of the platform, damage RISEC infrastructure, and catch on anchor and electrical cables that run from the floating platform to the riverbed.

A river surface debris diversion system—the RDDP—was deployed and tested at the Tanana River Test Site located at Nenana, Alaska. The RDDP system consists of a large (1360 kg) anchor connected to a mooring buoy (1.2 m diameter by 1.9 m length cylinder with a 1.9 m length conical section on the anchor chain end), which is in turn connected to the downstream surface debris diversion platform. The RDDP system has only a single high-capacity anchor chain extending from the riverbed to the mooring buoy. All other lines extend downstream from the mooring buoy parallel to the water surface (e.g., the RDDP and any RISEC floating platforms), reducing the number of potential locations where debris can accumulate.

The mooring buoy's constant movement in the river current creates an unstable site for the accumulation of debris, and the buoy's large buoyancy makes it difficult for debris to override the buoy. Consequently, the mooring buoy provides a strong first defense against surface debris by causing large debris objects that ride up its nose to slide off and become reoriented lengthwise, parallel to the current flow direction. Debris that is oriented with its long direction parallel to the current is easier for the RDDP to divert than debris that is crosswise to the current.

The RDDP, with two pontoons connected at their upstream ends such that their separation angle can be adjusted, was designed and tested as a way to protect surface-deployed RISEC devices from surface debris. The RDDP can accommodate either a cylindrical debris sweep with a radius of 1.1 m or a sharp-angled bow with an apex angle of 62 degrees.

Direct debris impact tests on the RDDP demonstrated that the cylindrical debris sweep with a surface cover of high-density plastic for creating a smooth sliding surface with reduced friction is very effective at diverting debris from the front of the RDDP to the pontoon surfaces. The debris sweep must be constructed to withstand significant debris impact forces. Forces for direct impact tests exceeded 6 kN, and maximum forces from natural debris impacts exceeded 3 kN. The sharp-angled front end did divert debris, but was much less effective than the debris sweep.

The opening angle between the RDDP pontoons has a significant effect on the ability of the pontoons to divert debris around the RDDP, as the force from water current pushing debris into the pontoons increases with increasing pontoon opening angle. The force from water current acting to clear debris from the pontoons' surfaces decreases with increasing pontoon opening angle. Debris can become pinned against the RDDP at pontoon opening angles greater than about 58 degrees. Larger opening angles can result in debris counter-rotating (rotating counterclockwise with respect to the river's right bank) under the RDDP, especially tree trunks that are twisted or are heavily covered with branches that extend below the bottom of the pontoons. Such counter-rotation can result in debris objects rotating or sliding under the pontoons.

Once debris has been diverted from its original path around the RDDP to a new path outside the "protected" flow paths, the debris generally remains clear of the RDDP's protected zone. The new flow path of the debris is generally parallel to the RDDP protected flow paths. Upwelling behind the debris sweep creates a surface wake that works to prevent debris from moving into the wake zone. River turbulence and overall current direction change due to being in proximity to a river bend can move debris across the river channel. This effect is not significant in a relatively straight reach of river, such as that used in our tests. River turbulence may nudge debris into the RDDP's protected current flow paths if it can overcome the RDDP's wake effect.

The ADCP measurements made behind the RDDP were unable to detect changes in the river current caused by the RDDP. The wide variability in river flow masked any signal of the RDDP's wake. Quasi-stationary ADCP measurements detected a decrease in the northward directed near-surface velocities as well as an increase in the westward directed near-surface velocities in the RDDP's wake. These changes were attributed to the presence of the RDDP. Changes in river flow direction were negligible several meters distant from the RDDP.

The RDDP system performed well at diverting river surface debris during the direct debris impact tests and during periods where the RDDP was left unattended for prolonged periods. The RDDP's performance can be further improved by covering the pontoon surfaces with a hard plastic sheet, which will reduce friction and provide a smooth contact surface for debris. Increasing the pontoon's draft will reduce the probability that debris objects can counter-rotate under the RDDP. Moving the safety railing from the outside to the inside of the pontoons reduces the probability of a debris object branch catching on a railing stanchion.

Reducing the inertia of the RDDP debris sweep and operating the RDDP with pontoon opening angles less than 40 degrees will improve the RDDP's ability to clear and divert debris. Increasing the RDDP pontoon draft will reduce the probability of debris counter-rotating under the pontoon. Attaching the RDDP to a downstream RISEC device will

increase its effective inertia to prevent large-momentum debris objects from rotating the RDDP around its mooring anchor point. A RISEC floating platform can be further protected by placing sheathing between the RDDP and a downstream RISEC platform to prevent debris from drifting into the RDDP protected current flow paths.

The RDDP system can provide a RISEC device deployed from a floating platform with effective protection from river surface debris. The RDDP is not designed to divert subsurface debris moving in the river. Further work is needed to understand the prevalence of subsurface debris to determine the probability of subsurface debris impacting a RISEC device and to guide concepts for protecting RISIC devices from subsurface debris.

References

ACEP. 2014a.AHERC Different Types of Natural Debris. http://youtu.be/I_L-rT1r13c.

ACEP. 2014b. AHERC Log Throwing. http://youtu.be/AQdb5uaZgmY.

ACEP. 2014c. AHERC RDDP Rear View of Log Being Diverted. 2014. http://youtu.be/Q_w9ASK9Ypo.

ACEP. 2014d. AHERC Log Rolling Under RDDP Pontoon. http://youtu.be/abGuxGk3FC0.

ACEP. 2014e. AHERC Fixed Apex. http://youtu.be/JVrj6fKsG-M.

ACEP. 2014f. AHERC Cotton Wood. http://youtu.be/zpuuB-uAhiA.

ACEP. 2014g. AHERC Debris Being Diverted at Both Sides. http://youtu.be/n_QEgVkXsnU.

ACEP. 2014h. AHERC Balancing Log. http://youtu.be/2Z-l_efgwZA.

ACEP. 2014i. AHERC Log Throwing. http://youtu.be/W-WFmLVPHzE.

Bradley, J., Richards, D., and Bahner, C. 2005. *Debris Control Structures – Evaluation and Countermeasures.* Salem, OR: U.S. Department of Transportation: Federal Highway Administration.

Danker, A.J., and Rosenfeld, A. 1981. Blob detection by relaxation. *IEEE Transactions on Pattern Analysis and Machine Intelligence*, 3(1): 79–92. doi:10.1109/TPAMI.1981.4767053.

Duvoy, P., and Toniolo, H. 2012. HYDROKAL: A module for in-stream hydrokinetic resource assessment. *Computers & Geosciences*, 39 (February): 171–181. doi:10.1016/j.cageo.2011.06.016.

Johnson, J.B., and Pride, D.M. 2010. River, Tidal, and Ocean Current Hydrokinetic Energy Technologies: Status and Future Opportunities in Alaska. Alaska Center for Energy and Power, 32 pp.

Johnson, J.B., Toniolo, H., Seitz, A.C., Schmid, J., and Duvoy, P. 2013. Characterization of the Tanana River at Nenana, Alaska, to Determine the Important Factors Affecting Site Selection, Deployment, and Operation of Hydrokinetic Devices to Generate Power. Alaska

Center for Energy and Power, Alaska Hydrokinetic Energy Research Center, Fairbanks, AK, 130 pp. http://www.uaf.edu/files/acep/2013_8_8_HKD_report_with_appendices.pdf.

Lang, V., Belyaev, A.G., Bogaevsici, I.A., and Kunii, T.L. 1997. Fast algorithms for ridge detection. *In:* Proceedings of the 1997 International Conference on Shape Modeling and Applications, pp. 189–197. doi:10.1109/SMA.1997.634896.

Pelunis-Messier, D. 2010. YRITWC Ruby Hydro_Sinking Turbine July 6, 2010. Youtube.com, Uploaded July 8, 2010. http://www.youtube.com/watch?v=57OA3svudvY.

Toniolo, H. 2013. RDDP influence on the hydrodynamic river conditions. Contribution to final project report: Eagle Hydrokinetic Project (01198-00-UAF G6078). Unpublished University of Alaska Fairbanks internal report, 12 pp.

Torre, V., and Poggio, T.A. 1986. On edge detection. *IEEE Transactions on Pattern Analysis and Machine Intelligence,* PAMI-8(2): 147–163, March. doi: 10.1109/TPAMI.1986.4767769.

Trajković, M., and Hedley, M. 1998. Fast corner detection. *Image and Vision Computing*, 16(2): 75–87. doi:10.1016/S0262-8856(97)00056-5.

Tyler, R.N. 2011. River Debris: Causes, Impacts, and Mitigation Techniques. Fairbanks, Alaska Center for Energy and Power, 33 pp. http://www.uaf.edu/files/acep/2011_4_13_AHERC-River-Debris-Report.pdf.

Appendix A: Nenana Tanana River Test Site Mooring System

The mooring system is comprised of the following components:

- 3000 lb (1360 kg) Flipper Delta patent drag embedment anchor with anchor shackle (Figure A1)
- Connection between anchor chain and anchor shackle (Figure A2)
    - 7/8″ × 4′ (22 mm × 1.2 m) wire rope choker (Internal Wire Rope Core Extra Improved Plow Steel, IWRC XIP) with thimbles passed through anchor shackle
    - Choker is secured with two 5/8″ galvanized shackles to a grade 100 master link
    - Master link is secured to the anchor chain with a 7/8″ (22 mm) galvanized shackle
- Anchor chain
    - Two shots (90′, 27.4 m) 7/8″ (22 mm) grade 2a stud link chain
    - The two shots of chain are connected with a grade 3a Kenter link
    - The anchor chain is connected to the mooring buoy with a 3/4″ (19 mm) galvanized shackle
- Lifting pendant to facilitate anchor removal
    - 5/8″ × 60′ (16 mm × 18.3 m) galvanized wire rope with thimble eye secured to the anchor lifting eye with a 5/8″ (16 mm)
    - A standard eye on the other end of the pendant is secured to the anchor chain with a 3/8″ shackle
- Mooring buoy (Figure A3)
    - Comprised of cylinder with a diameter of 46″ and length of 74″ with a 46″ cone on the anchored end
    - A 3″ diameter steel pipe placed through the cylinder on its axis has a ring on the cone end to accommodate a shackle that secures the anchor chain to the buoy. The other end of the pipe extends 20″ past the end of the cylinder and is configure in the shape of cross to be used as a mooring bitt
    - The tension forces resulting from a device being moored to the buoy are applied to the pipe rather than the sides of the buoy
- Mooring lines used, AmSteel® Blue, Dyneema® fiber
    - 1″ × 60′ (25 mm × 18 m) AmSteel® Blue
    - 1/2″ × 250′ (13 mm × 76 m) AmSteel® Blue
- Quick release on RDDP
    - Sea Catch Model TR8

Table A1. Mooring system component capacities.

	Working Load Limit lbf (kN)	Proof Load lbf (kN)	Break Strength lbf (kN)
7/8″ (22 mm) Wire rope choker (a)	30,000 (133)		78,000 (345)
5/8″ (16 mm) galvanized shackle (b)	6,500 (28.9)	14,300 (63.6)	39,000 (174)
V10 Master link, Grade 100 (c)	39,100 (174)		
7/8″ (22 mm) galvanized shackle (b)	13,000 (57.8)	28,600 (127)	78,000 (347)
7/8″ grade 2a anchor chain (d)		46,000 (205)	64,400 (286)
Kenter link grade 3a (d)		64,400 (286)	91,800 (408)
3/4″ (19 mm) galvanized shackle (b)	9,500 (42.3)	20,900 (93.0)	57,000 (254)
5/8″ (16 mm)wire rope lifting pendant (d)	7,800 (34.7)		
1″ AmSteel® Blue	21,800 (97)		109,000 (485)
1/2″ AmSteel® Blue	6,800 (30)		34,000 (151)
Sea Catch TR8 Quick Release (e)	9,574 (42.6)		47,870 (213)

Sources of load capacity data:
(a) West Coast Wire Rope, Seattle WA, www.wcwr.com
(b) Working Load Limit (WLL) marking on shackle, proof load = 2.2 × WLL, break strength = 6 × WLL
(c) Peerless Industrial Group, Winona MN, www.peerlesschain.com
(d) Washington Chain and Supply, Seattle WA, wachain.com
(e) McMillan Design, Inc., Gig Harbor, WA, www.seacatch.com

Figure A1. Anchor prior to deployment.

Figure A2. Anchor shackle, wire rope choker, shackles and master link.

Figure A3. Mooring buoy prior to deployment.

Appendix B: Independent Power Supply Box Manual

Manual for the Nenana Imaging System Solar Panel Power Supply Jobox

Marc Mueller-Stoffels, mmuellerstoffels@alaska.edu
Elliott Mitchell-Colgan, e.mitchell.colgan@alaska.edu
Kelsey Boyer, kjboyer@alaska.edu

July 3, 2012

1

1 First Things First

Figure 1: Oh look, there's a log book in the box!!! **USE IT** to keep track of fuel and oil consumption (first indicators that something is wrong), and to record anything else out of the ordinary. Initial your entries.

Contents

2 Independent Power Supply Box Inventory

The following hardware and items should be in the box. If they are not they should be restocked.

2.1 Essential Hardware

Compare to Figure 1 and Figure 2.1.

- Honda Eu2000i Generator (1)
- Trojan 6 V 420 Ah Lead-Acid Batteries (2)
- 60 A DC Fuse (1)
- 5 gal Metal Gas Cans (2)
- 600 CFM Fan (1)
- Iota DS-55 12 V Battery Charger (1)
- Iota Q4 Battery Charge Controller (1)
- 150 W Samlex DC-AC Inverter (1)
- AC Transfer Switch AMPS AND MANUFACTURER (1)
- Short Ratchet Straps (2)
- AC Input On/Off Switch (1)
- 115 V 1500 W (max) Outlets (4)
- 115 V 150 W (max) Outlets (2)
- 190W Canadian Solar PV Panel
- 10A DC Breaker and Breaker Box
- Sunsaver MPPT Charge Controller

Figure 2: Box setup: Fuel supply to the left, Fan in the back left, Batteries in the front, Power electronics on the back panel, Generator on the far right.

2.2 Maintenance and Back-up Equipment

- Manuals for Generator, Battery Charger, Inverter, AC Transfer Switch, Solar Charge Controller.
- Datasheet for the Solar Panel.
- 2 qt 10-W30 Engine oil
- 2 CR5HSB Spark Plugs
- 2 ratchet straps
- Flex hose funnel for refueling
- Small funnel for oil changes
- 148pc Mechanics tool kit
- 9 1/2" Pump Pliers
- 60 A DC fuse
- GE Multimeter
- Miscellaneous Unistrut Hardware
- 3/4" Wrench (for Unistrut bolts)

Figure 3: Power panel setup: Top left: Battery charger and controller (small black box on top); Top right: DC-AC inverter; To the left: 13 A 115 V outlets and AC power on/off switch; Right: 150 W 115 V AC outlets; Bottom Right: SunSaver Solar Charge Controller.

3 Generator and Fuel System

The Independent Power Supply (IPS) is mainly powered by a Honda Eu2000i generator with a modified fuel system. The fuel line has an external intake to accommodate connection of auxiliary fuel tanks.

For general generator operation please refer to the Honda Manual.

Positions on the generator used herein use the front panel (electrical outlets) of the generator as reference point.

3.1 Operating the Generator using the Auxiliary Fuel Tanks

3.1.1 Refueling

In order to be able to use the external fuel tanks with a relatively long fuel line the following procedure needs to be followed: (i) with the external fuel valves in the OFF position fill both auxiliary fuel tanks to similar levels; (ii) make sure the air line valve above the fuel tanks is open; (iii) make sure that there is some fuel in the generator's internal tank, a 1/4 tank is enough; (iv) IMPORTANT: make sure the air valve on the generator's fuel cap is in the OFF position. If the generator fuel cap is left on the ON position the fuel system will not generate enough suction to draw fuel from the auxiliary tanks.

3.1.2 Starting the Generator

Before you start the generator make sure that (i) no load is connected to it by turning the AC switch (Fig. 2.1) on the electrical board to the OFF position; (ii) make sure that the 'Eco-Switch' at the front of the generator is in the OFF position.

To start the generator (i) open the two valves on the external fuel line; (ii) turn the ON/OFF switch, located on the left panel towards the bottom/front, to the ON position; (iii) pull the choke, located on the left panel towards the top back, towards the front of the generator; (iv) pull the recoil starter.

Once the generator is running return the choke to the back position. Wait until a green LED illuminates at the front panel of the generator. Turn the AC switch to the ON position and turn the 'Eco-Switch' to the ON position. Note, it is best for the engine to follow the above order of flipping switches.

3.1.3 Stopping the Generator

Return the ON/OFF switch to the OFF position. Close the two valves on the external fuel line.

Note, the internal fuel shut-off is built into the ON/OFF switch.

3.2 Generator Maintenance

The Honda Eu2000i is equipped with a low oil sensor. Low oil conditions will shut off the generator and briefly illuminate the red oil warning LED at the front of the generator. In cold weather (AK cold that is), the generator might shut off due to a low oil sensing shortly after start-up although there appears to be enough oil in the system. This condition will require a few restarts and a few minutes runtime while the engine is fully choked. If the condition persists, an oil change might be in order.

3.2.1 Changing the Oil

An oil change is officially required every 100 hours of run time. Since we are running the generator at or below half load, an oil change every 250 hours will suffice.

Always use warm (room temperature) oil when refilling the generator. Failure to do so will over-pressurize the oil system once the oil heats and expands, which can lead to severe damage.

1) Turn off both valves on the auxiliary fuel line.
2) Disconnect the auxiliary fuel line.
3) Loosen the strap holding the generator.
4) Carefully pull the generator **straight** back until the external exhaust pipe comes free of the wall mounted pipe.
5) Take the generator out of the box.
6) With a coin or a screw driver loosen the screw holding the side panel in place.
7) Carefully move the side panel out of the way. You will have to slowly feed the auxiliary fuel line through it.
8) Follow the instructions in the Honda Eu2000i service manual regarding oil changes. Perform the oil change over the oil pan included in the box. Use the small blue funnel to fill oil into the generator and old oil into an empty oil container.
9) Follow steps 7 - 1 in reverse order.

3.2.2 Changing the Spark Plug

If the generator is running rough or won't start it might be time to change the spark plug. In order to do so follow steps 1 through 5 in the Oil Change Section and then the service manual. It is recommended to change the spark plug every year.

4 Electrical System

The IPS is equipped with two 6V 420 Ah open lead-acid batteries connected to form a 12 V 420 Ah DC power supply. Figure 4 gives an overview of the components.

The generator feeds into an AC switch which can be used to isolate the system from generator AC power. Behind the switch are four AC outlets. These can be loaded to a total of 1500 W permanent power. To find the power draw for a piece of equipment multiply the input current given for the equipment by 115 V.

The AC fan and the battery charger should be connected to these outlets. **Never connect the battery charger to the other outlet behind the AC transfer switch**.

The fan needs to be running if the generator is in operation or the batteries are being charged. **Open lead-acid batteries generate hydrogen gas during charge cycles. Hydrogen is extremely volatile and can cause explosions resulting in severe injury or death. Always ventilate the batteries when charging.**

From the four AC outlets a connection runs to the automatic AC transfer switch. This switch senses if external (from the generator) power is available. If this is the case all AC outlets are powered using the source. Else power is drawn from the DC to AC inverter.

The battery charger has a 30 A fused AC input and DC 0/2 gauge connections to the batteries. **Warning: during charging the cables from the battery charger to the batteries carry up to 55 Amps of current. Make sure the battery charger is OFF, that is disconnected from AC power, before disconnecting DC wiring.**

The batteries feed the DC to AC Inverter. The inverter has an ON/OFF switch on the left side towards the bottom. This can be left in the ON position at

all times. **If disconnection the batteries, turn off the inverter**. This prevents damage caused by surges in current from the batteries the instant they are plugged in.

The positive connection at the battery is protected by a 60 A DC fuse. A replacement fuse is in the box.

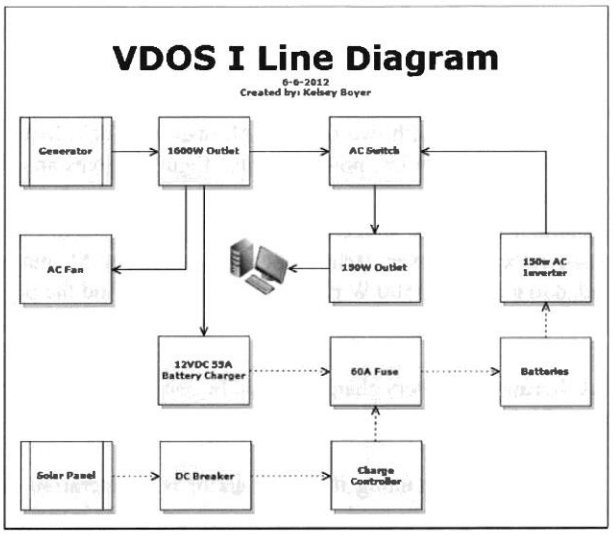

Figure 4: Line diagram. Black solid lines denote AC connections. Black dotted lines denote DC connections.

5 Storage

5.1 Short-term storage

For short-term storage (under 60 days) close all valves except the air vent for the auxiliary fuel tank. Disconnect the batteries from the electrical system by unplugging the DC cable connectors.

5.2 Long-term and winter storage

Batteries can freeze resulting in severe damage and possible acid spills.

For long-term storage disconnect the DC cables at the batteries. Remove the batteries from the box an store in a heated, dry space. Ideally the batteries are connected to trickle charger. **Remember each single battery is a 6V block.**

Remove all fuel from the system. Please see section 8 on page 13 for information on disassembling and assembling the Jobox.

6 Solar Panel Power Supply

6.1 Hardware Overview

The hardware involved in the solar panel battery-charging system is basically comprised of the solar panel, the solar-battery charger, and the batteries themselves.

* 190W Canadian Solar CS5A Monocrystalline Solar Panel (1)
* SunSaver MPPT 150 Solar Charge Controller (1)
* Breaker Box with a 10A DC Breaker

6.2 Maintenance for Solar Panel System

The solar panel does not require maintenance in particular other than wiping off the dust from the glass casing as often as possible. The batteries, however, should be checked for charge and charged until full if they are not, and deionized water should be added until it reaches 1/8 of an inch below the top of the plastic case. Please consult a guide to maintenance on Flooded Lead-Acid batteries.

6.3 Setting the Angle of the Solar Panel

At different times of the year, the sun takes different trajectories through the sky. In order to absorb the most sun as possible, the solar panel should be tilted at different angles by moving the green unistrut brace to preset studs in the unistrut. The studs are **marked by month on the unistrut**. The optimum angle by month are as follows in Table 1.

March	25°
April	33°
May	41°
June	48°
July	41°
August	33°
October	25°

Table 1: Optimum Solar Panel Angle (from the normal) by Month

6.4 SunSaver MPPT Solar Controller Usage

The settings on the SunSaver are correct for the Nenana shore-side imaging application. If the system is changed, please refer to the information below and the SunSaver manual.

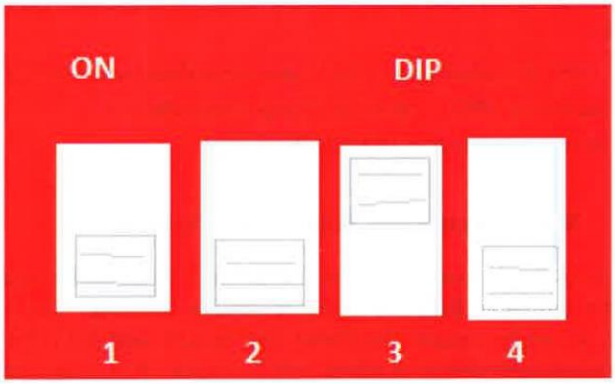

Figure 5: The DIP Switch should look like this.

The charge controller has settings for different types of batteries, and changing the battery architecture (now it's FLA) may require the jumper (looks sort of like a metal guitar pick with holes in it). That can be found inside of the SunSaver box in the Jobox. For the current system, the SunSaver's DIP switch settings should be like figure 5 above. The ports labeled "Load" should be left unplugged, for we are only charging batteries. The **SunSaver User's Manual** can be found in the Jobox for further information.

If the **batteries are changed**, consult the **SunSaver Manual** in the box to ensure that the jumper and 1st DIP switch are correct.

7 Power Loss During Runtime

The solar panels may not always be able to provide power for the laptop. If the system experiences complete loss of power, a full system restart is required. This involves restarting the computer, checking to be sure the hard drives are operational and that the computer can sense them (check my computer), and that the imaging Matlab software starts again. Also, check the inverter to see if turning it off and then back on is necessary (is the "fault" light on?).

8 Transporting the Jobox

For ease of transportation, the solar panel are mounted such that they will slide down against the back side of the solar panel. Disassembly and reassembly are designed to be relatively easy and quick. However, this is a **2 person job** in order to ensure the safety of the solar panel. Also, please leave all of the nuts and bolts near the holes they were attached to in order to ensure that there are enough parts and to avoid confusion as to the correct state of the hardware.

8.1 Assembly and Disassembly of Solar Panel

1. This is the VDOS I folded down and prepared for transport. This tutorial will guide you through assembling the solar panel. For disassembly, please follow these steps very closely in reverse order (7-1)

14

2. Disconnect the green brace from the unistrut making sure to leave the bolt and nut in the brace and not the unistrut.

3. Next, attach the spare braces to the solar panel at the points indicated in the photo.

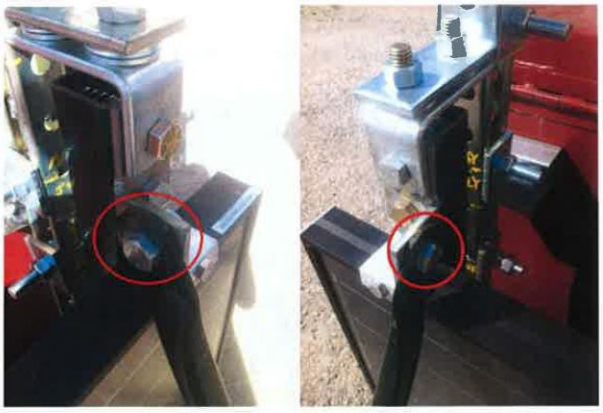

4. Disconnect Solar Panel brackets from Unistrut support at the indicated points, take precautions so that the panel does not fall onto the ground after disconnecting from the support.

5. Attach the lower support braces by swinging up the bottom of the solar panel as indicated in the photo and attaching the bolts in the indicated holes.

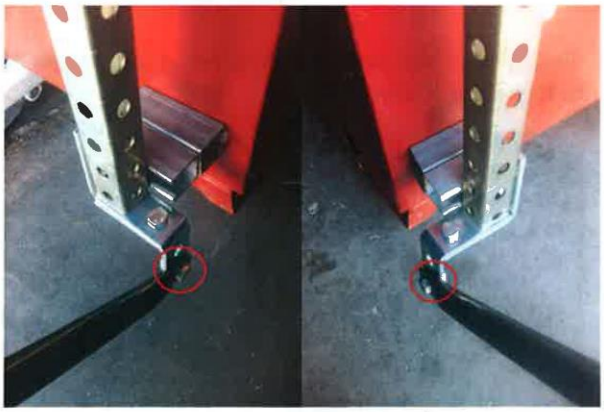

6. Attach the upper green braces to the unistrut taking note to attach the panel to the appropriate stud depending on the current month of operation. Solar panel angle should be adjusted to the preset studs depending on current month.

7. Finally, attach the cross brace to the preset studs. Extra bolts and nuts can be found in the JoBox if needed.